



New graphene oxide-safranin modified@polyacrylonitrile membranes for removal of emerging contaminants: The role of chemical and morphological features

Tauany de Figueiredo Neves^a, Natália Gabriele Camparotto^a, Everton Augusto Rodrigues^a, Valmor Roberto Mastelaro^b, Renato Falcão Dantas^a, Patrícia Prediger^{a,*}

^a Limeira School of Technology, University of Campinas, PO Box 456, 13484-332 Limeira, S.P., Brazil

^b São Carlos Institute of Physics, University of São Paulo, PO Box 369, 13566-590 São Carlos, S.P., Brazil

ARTICLE INFO

Keywords:

Functionalized graphene oxide
Adsorption process
Ultrafiltration
Propranolol
Surfactants
Dyes

ABSTRACT

Polymeric membranes incorporated with graphene oxide (GO) are promising materials for treating contaminated water, but few studies relate the chemical and morphological changes in the polymer matrix and permeation flux with the membrane performance. In this study, new hydrolyzed polyacrylonitrile (hPAN) membranes containing GO (hPAN@GO) and GO modified with the cationic dye safranin (hPAN@GO-SF), with varying nanomaterial content of 2–10%, were synthesized, fully characterized and applied to the removal of emerging contaminants (ECs) from water. The incorporation of GO-SF in the polymeric matrix reduced the membranes surface roughness, modified the size and shape of the sublayers macrovoids and increased the materials hydrophilicity, providing better adhesion of ECs. hPAN@GO-SF reached removal capacities of 200.6, 154.8, and 191.1 mg.g⁻¹ for propranolol drug, benzalkonium chloride surfactant and methylene blue dye, respectively, in batch assays both at 100 mg.L⁻¹. Ultrafiltration experiments revealed a high water flux up to 183 L.m⁻².h⁻¹ and rejection rates and removal capacities for the cationic dyes basic blue 26 (84% ~ 242.6 mg.m⁻²) and basic green 4 (90% ~ 237.4 mg.m⁻²) by hPAN@GO-SF membranes at concentration of 10 mg.L⁻¹. Density functional theory calculations, batch experiments in saline medium and post adsorption XPS analysis indicated that cation-exchange, electrostatic and π - π interactions are the main mechanism and that the differences in the solute flow profile favor or limit adsorbent/adsorbate interactions according to the contaminant. The results show that polyacrylonitrile membranes containing GO functionalized by SF have potential to remove multiple ECs from water in batch assays and ultrafiltration.

1. Introduction

Called emerging contaminants (ECs) any synthetic or natural substances with potential to adversely affect the environment and human health, pharmaceutical drugs, surfactants and dyes are relevant examples of this class of compounds [1]. Nowadays, the recurrent presence of ECs in water has become one of the main global problems [2] and expose the inefficiency of water conventional treatments employed [3]. In this context, numerous techniques have been developed to mitigate the pollution of water bodies [4–7], including membrane separation [8].

An advanced water treatment technique that allows the continuous operation of the process, membrane separation has its functionality related to the mechanism of rejection of the film to aquatic contaminants

[8]. Nanofiltration (NF), a membrane separation technology, is the most used technology for water treatment and is based on size rejection [9]. However, the small pore size of the membrane reduces the flow in the process. Seeking to improve this parameter, several studies have recently used loose NF membranes [10] or tight ultrafiltration (UF) [11] in the treatment of contaminated water, which has its mechanism rejection based on electrostatic effect.

Polyacrylonitrile (PAN), a synthetic polymer obtained from the polymerization of acrylonitrile, is commonly used as membrane for gas separation [12], air filtration [13] and water NF [14] and UF [15]. It is an inexpensive material containing nitrile groups that enable different interactions between the polymer and chemical pollutants, due to presence of electron-rich and poor centers [16]. Still, PAN UF

* Corresponding author.

E-mail address: prediger@unicamp.br (P. Prediger).

<https://doi.org/10.1016/j.cej.2022.137176>

Received 2 March 2022; Received in revised form 2 May 2022; Accepted 22 May 2022

Available online 24 May 2022

1385-8947/© 2022 Elsevier B.V. All rights reserved.

membranes are rarely used directly for the removal of water contaminants such as dyes, surfactants or pharmaceutical drugs due to the pore size, slightly larger than contaminant molecules, low flow rate and surface fouling [17]. There are methodologies to mitigate these limitations of PAN UF membranes: (1) chemical modification of the membrane surface through alkaline hydrolysis [18], amination [19], oxidation [20] or UV light modification [21]; (2) membrane integration with other separation mechanisms such as adsorption [14], in these cases nanoparticles can be integrated into the polymer solution before the fabrication of the membrane [22] or as a coating layer on its surface [23].

In this regard, the use of graphene oxide (GO) in the preparation of PAN UF membranes emerges as a possible way of improving the filtration process. GO, a nano-adsorbent obtained by the incomplete oxidation of graphite, can chemically and physically influence the properties of membranes. Because it has functional oxygenated groups (for example, hydroxyl, carboxyl and epoxy) in the chemical bias, GO can interact with microorganisms and pollutants through hydrophobic, electrostatic and π -stacking interactions, among others [24]. Regarding morphological issues, GO imparts surface defects to membranes such as changes in pore size and distribution [25], roughness [26], and hydrophilicity [27], which can enhance the PAN UF characteristics such as selectivity, anti-fouling and hydrophilicity, leading to higher water flux [28].

Several studies have evaluated the potential of GO membranes to remove organic compounds from water by filtration [27] and these membranes have also been used in batch adsorption [29]. Juengcharoonpon et al. [30] studied the adsorption of the antibiotic trimethoprim on GO-carboxymethylcellulose films coated in polyethylene terephthalate in batch and continuous flow processes. The maximum adsorption capacity of the material was $209.8 \text{ mg}\cdot\text{g}^{-1}$ and $175.9 \text{ mg}\cdot\text{g}^{-1}$ for the batch and fixed bed tests, respectively. According to the authors, this increase in the adsorption potential of the membrane when used in a batch process may be associated with the longer contact time between adsorbent/adsorbate, which influences the physicochemical interactions of the film with the contaminant.

Despite the potential incorporation of GO into PAN membranes, the removal capacity of these new materials is expressive for cationic contaminants but ineffective for anionic compounds, mainly due to the incorporation of oxygenated groups of GO in the PAN polymer matrix [28]. In this scenario, the incorporation of cations in adsorbents emerges as a new methodology to broaden the removal spectrum of PAN membranes with GO [31], as reported by Zhang et al. [32]. According to the authors the adsorption of anionic dye methyl orange II (MO-II) onto GO surface was enhanced in the presence of cations such as methylene blue dye (MB) and lead ions (Pb^{2+}). Following this logic, the question arose whether the insertion of cation-functionalized GO in the PAN membrane enhance the performance and membrane selectivity in the removal of anionic and electron-rich contaminants from water.

Several studies reported in the literature, using preparation methodologies such as vacuum filtration and layer-by-layer assembly processes, have already explored the potential of membranes based on GO and modified GO in the removal of ECs in water [33-36]. However, little is addressed how the incorporation of these adsorbents into the polymer matrix influences the membrane separation potential. Therefore, this study aimed to evaluate how the chemical and morphological features influence the selectivity of PAN UF membranes incorporated with modified GO in the removal of ECs through batch and ultrafiltration processes. We prepared new hydrolyzed PAN (hPAN) membranes containing GO (hPAN@GO) and GO modified with the cationic dye safranin (hPAN@GO-SF), varying the nanomaterial content by 2, 4, 6, 8 and 10%. The new membranes were fully characterized by AFM in liquid medium, SEM, FT-IR, XPS, zeta potential, water contact angle and microtomography to evaluate their chemical and morphological properties according to the content of incorporated nanomaterial. hPAN@GO and hPAN@GO-SF membranes were used in the removal of pharmaceutical drugs, surfactants and dyes from water, through batch and ultrafiltration tests. Density functional theory (DFT) calculations of

the contaminants' molecules were carried out aiming at a deeper understanding of the interactions between adsorbent/adsorbate and a proposal of the main mechanism is presented. To the best of our knowledge, it is the first time that GO chemically modified with cationic molecule has been incorporated into the PAN membrane and its influence on membrane characteristics has been systematically studied and related to the performance in removal ECs.

2. Experimental section

The experimental section of the work can be found in the [supporting information](#) file attached. This topic describes the chemical reagents and materials used in the synthesis of the new membranes (Section S1.1), the methodologies addressed for the preparation of materials (Section S1.2), descriptions of the characterizations used (Section S1.3), the procedures for the removal tests of contaminants (Section S1.4) and the descriptions of the theoretical density functional study (DFT) (Section S1.5).

3. Results and discussion

3.1. Preparation of membranes

The synthesis of hPAN@GO-SF membranes was carried out in two steps (Fig. 1). Initially the safranin dye (SF) was attached to GO via amidation reaction followed by its incorporation to PAN polymer generating the functionalized membrane that was partially hydrolyzed giving rise to hPAN@GO-membranes.

3.2. Characterizations

The graphene oxide employed in this work was characterized in our previous work [37]. According to AFM analyses the adsorbent sheets had a lateral size of $0.9\text{--}5.2 \mu\text{m}$ and average thickness of 1.2 nm [37], suggesting the presence of GO monosheets and BET analysis estimated that the synthesized adsorbent had a surface area of $351 \text{ m}^2\cdot\text{g}^{-1}$ [37].

3.2.1. Characterizations of GO-SF

3.2.1.1. X-ray diffraction (XRD). The diffraction patterns of graphite, GO and GO-SF are shown in Fig. 2(a). The data indicated that as the graphite oxidation and later, the functionalization of GO, the 2θ angle of the materials decreased, with the observed patterns being 26.6° , 12.5° and 9.6° , for graphite, GO and GO-SF, respectively. Applying the Bragg's law equation, the interlayer spacing of the materials increased significantly with the modifications, with graphite having a spacing of 0.3 nm , GO 0.71 nm and GO-SF 0.9 nm [38]. The increase in the interlayer spacing between GO and graphite indicates the presence of defects in the mineral's crystalline structure, suggesting the insertion of oxygenated groups generating GO [39]. In turn, the increase in interlayer spacing from GO to GO-SF suggests the insertion of SF in the structure, since the presence of phenazine units in GO increases the electrostatic repulsion between the material's nanosheets [7].

3.2.1.2. Fourier-transform infrared spectroscopy (FT-IR). The FT-IR spectra of GO, SF and GO-SF are shown in Fig. 2(b). The spectrum of GO reveals bands around 3437 , 1734 and 1632 cm^{-1} attributed to the presence of OH, ketone and carboxyl groups, respectively. The SF dye spectrum reveals a broad band at 3435 cm^{-1} referring to the presence of OH and another at 3198 cm^{-1} attributed to NH groups [40]. It is also possible to verify the presence of bands at 2930 and 2857 cm^{-1} referring to the symmetric and asymmetric stretching of CH units, respectively [7]. The band at 1646 cm^{-1} is attributed to the SF aromatic rings. The bands at 1612 , 1534 , 1494 and 1334 cm^{-1} refer to the N^+ cation, the heterocyclic rings, and the symmetric and asymmetric bending vibrations of the CH_3 groups, respectively [41]. The bands at 1194 and 1021

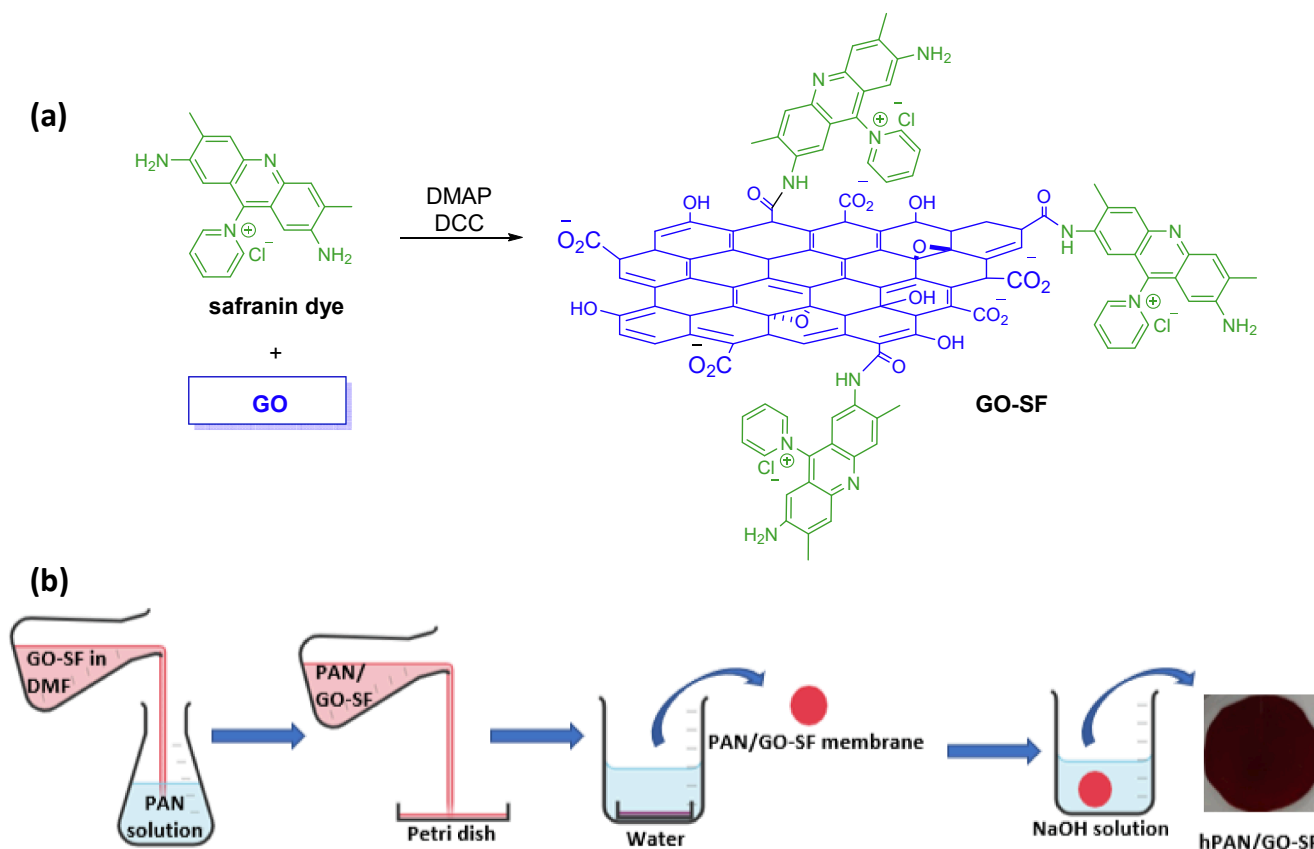


Fig. 1. (a) Synthesis of GO-SF; (b) Scheme for preparing hPAN@GO-SF membranes.

cm^{-1} are attributed to vibrations of the C-N bonds in amines [42].

The GO-SF spectrum has bands referring to the GO and SF functional groups, with some shifts. Young et al. [43] associated these changes in band shape and peak shifting with intermolecular interactions. For example, the broadband in the region of 3400 cm^{-1} , referring to the OH groups, shifted to 3428 cm^{-1} compared to the GO (3437 cm^{-1}) and SF (3435 cm^{-1}) spectra, suggesting the presence of hydrogen bonds between the hydroxyl and carboxyl of the adsorbent and the nitrogen groups of the SF. At 3200 , 2928 and 2851 cm^{-1} , it is possible to verify the bands of NH groups and of the symmetrical and asymmetrical stretches of CH units of SF, respectively. In 1729 and 1646 cm^{-1} are the bands attributed to the presence of ketones and carboxyl, respectively. A new band observed at 1657 cm^{-1} is attributed to the formation of the amide bond between GO and SF [7,44]. The other bands are similar to those found in the SF spectrum. Through the FTIR analysis, it can be concluded that we were successful in preparing the GO-SF.

3.2.1.3. X-ray photoelectron spectroscopy (XPS). The elemental composition of the materials and the high resolution spectra of GO and GO-SF are shown in Fig. 2(c-g). Analyzing the tabulated data obtained from the survey spectrum of the materials in Fig. 2(c), it was possible to observe that the GO had an elemental composition endowed only with carbon (C – 77.2%) and oxygen (O – 22.8%). While GO-SF had of C (78.1%), O (15.2%), nitrogen (N – 6.0%) and chlorine (Cl – 0.6%). The elemental composition obtained for the GO-SF indicated the insertion of SF in the GO, since the incorporation of the dye increased the carbon content present in the material, in addition to adding the N and Cl structure, characteristic elements of SF.

High resolution C1s spectrum for GO (Fig. 2(d)) revealed peaks centered at 284.8 eV (C- sp^3 /C- sp^2), 286.9 eV (C-OH) and 288.5 eV (O-C = O) [45,46]. For GO-SF, the high-resolution C1s analysis (Fig. 2(e)), in addition to the characteristic peaks present in GO, with N at the bands

286.9 eV (C-OH /C-N) and 288.5 eV (O-C = O/O = C-N) [47], showed a new peak centered at 287.5 eV associated with C = O/C = N bonds [48]. Furthermore, the high resolution N spectrum (Fig. 2(f)) of the material indicated two signals at 399.0 and 400.3 eV , referring to amine group (NH_2) and amide group (N-C = O), respectively [49].

3.2.1.4. Zeta potential. The zeta potential of GO and GO-SF, in the range of pH 4–10 is shown in Fig. 2(g). Both materials, had a negative surface charge in the range of evaluated pH. The GO-SF presented zeta potential (-7.41 to -25.8 mV) less electronegative than the GO (-14.9 to -45.1 mV). GO has several carboxyl (COOH), hydroxyl (OH) and epoxy (O) groups in the basal plane and on the edges of the nanosheets, which contribute to its electronegative character [50], while GO-SF has less electronegative surface charge due to insertion of the cationic dye SF in the GO domain. Thus, although the presence of SF incorporates phenazinium cations into the nanomaterial matrix, the intense presence of oxygenated groups in GO still maintains the surface charge of GO-SF with electronegative potential. Similar result was obtained in our recent study that reported electronegative potentials for magnetic composite based on chitosan and GO-quaternary ammonium salt [7].

3.2.2. Characterization of new membranes

3.2.2.1. X-ray diffraction (XRD), Fourier-transform infrared spectroscopy (FT-IR) and X-ray photoelectron spectroscopy (XPS). Fig. S1(a-d) show the XRD patterns and FT-IR spectra of the GO/GO-SF nanomaterials, the hPAN membrane and the incorporated membranes at levels ranging from 2 to 10% of nanoadsorbents. The hPAN@GO and hPAN@GO-SF spectra did not show relevant changes when compared to hPAN spectrum. This result was expected due to two factors: (1) The mass of adsorbents incorporated into the polymer matrix are small [51] and (2) XRD and FT-IR characterizations analyze the sample surface [52], and as

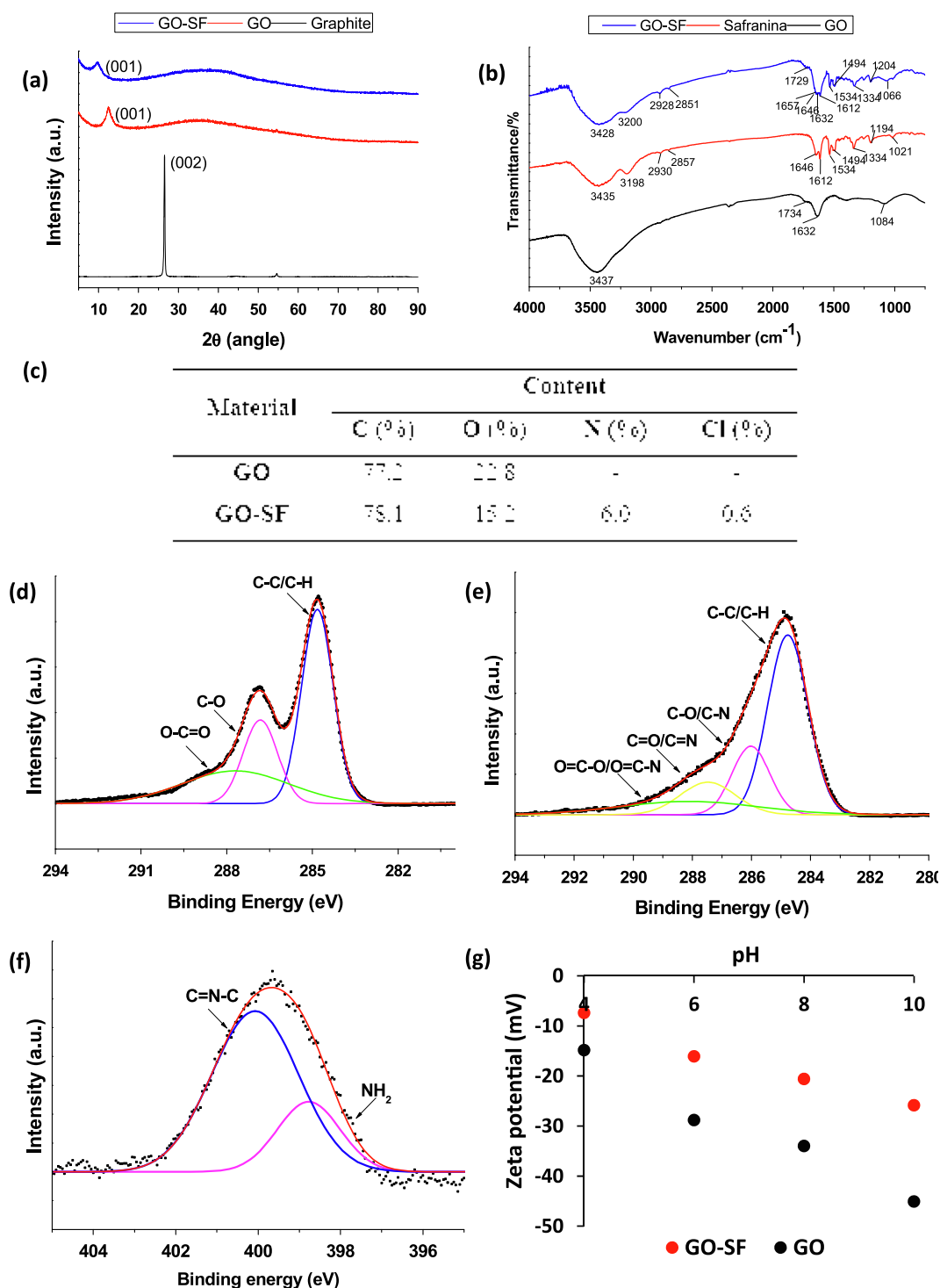


Fig. 2. (a) XRD pattern of GO-SF (blue line), GO (red line) and graphite (black line); (b) FTIR spectra of GO-SF (blue line), SF (red line) and GO (black line); (c) Data obtained for GO and GO-SF by XPS survey; (d) C1s high-resolution XPS spectrum of GO; (e) C1s high-resolution XPS spectrum of GO-SF; (f) N1s high-resolution XPS spectrum of GO-SF; (g) Zeta potential of GO-SF (red circle) and GO (black circle). 1:2.3 g mass ratio of GO:SF.

the adsorbent is incorporated into the PAN solution, GO and GO-SF are not present on the surface of the material.

The membranes elemental composition by XPS survey analysis and C 1 s and N 1 s high resolution XPS spectra for hPAN, hPAN@GO 6% and hPAN@GO-SF 6% are shown in Fig. 3(a-g). The tabulated data (Fig. 3(a)) obtained from the survey analysis show that hPAN had an elemental composition endowed with C (76.9%), N (11.3%), O (11.4%) and Na (0.3%), the last due to the alkaline hydrolysis [53]. The membranes incorporated with GO showed a similar elemental composition, however

an increase in the oxygen content was observed. In general, the more GO incorporated into the membrane, the greater its O content. The presence of GO-SF in membranes was confirmed by the increase in N content, as well as the appearance of chlorine in the elemental composition of materials. Both elements are characteristic of the SF dye.

High resolution C1s for hPAN (Fig. 3(b)) revealed peaks centered at 284.5 eV (C-sp³/C-sp²), 285.4 eV (C-N/C-O), 286.3 (C-O-C), 287.6 eV (C=O) and 288.8 eV (COOH), corresponding to the percentages of carbon bonds of 43.8%, 17.4%, 25.7%, 10.8% and 2.2%, respectively [54]. For

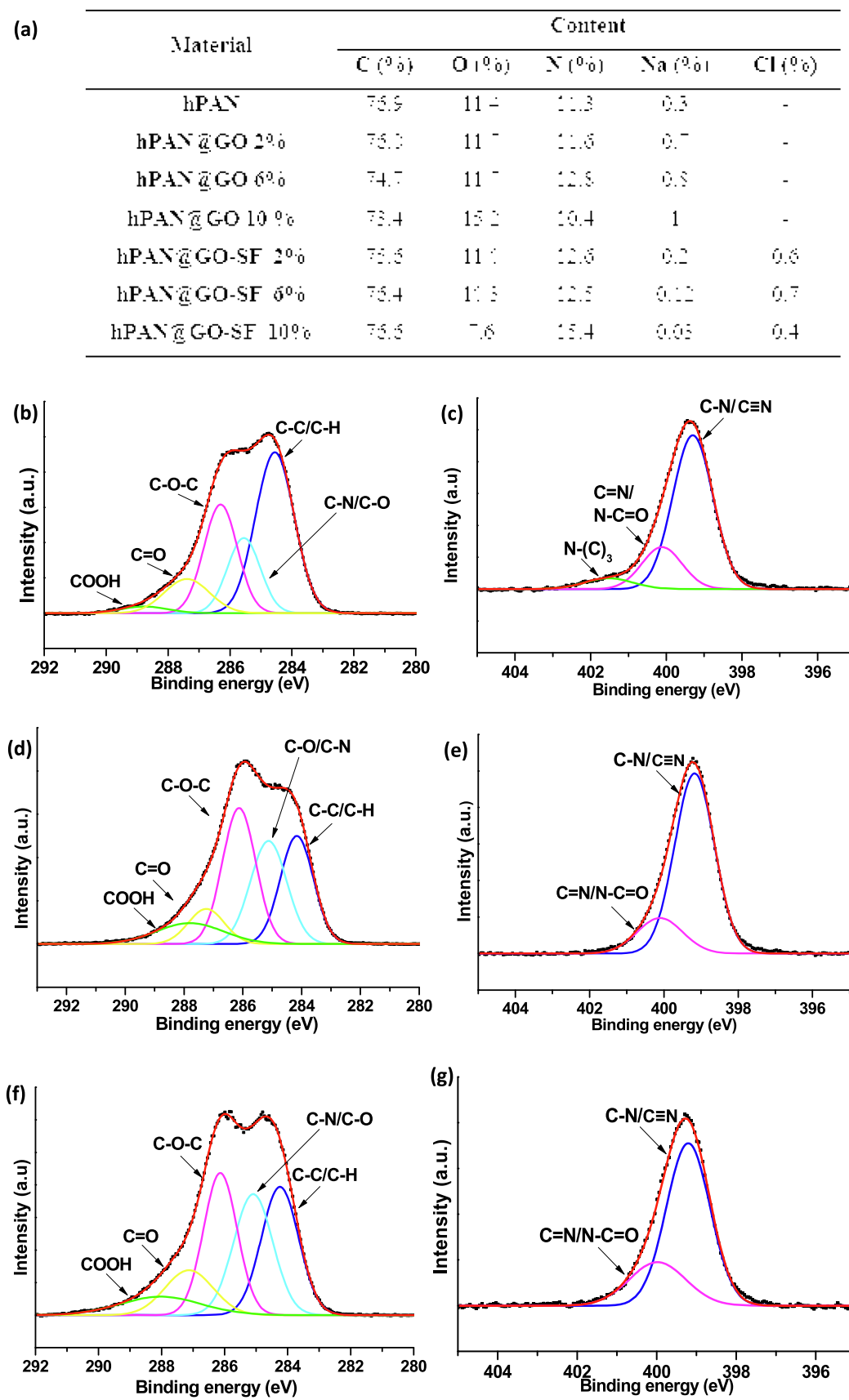


Fig. 3. (a) Data obtained for membranes by XPS survey; (b) C1s high-resolution XPS spectrum of hPAN; (c) N1s high-resolution XPS spectrum of hPAN; (d) C1s high-resolution XPS spectrum of hPAN@GO 6%; (e) N1s high-resolution XPS spectrum of hPAN@GO 6%; (f) C1s high-resolution XPS spectrum of hPAN@GO-SF 6%; (g) N1s high-resolution XPS spectrum of hPAN@GO-SF 6%.

the membranes containing GO and GO-SF, high-resolution C1s (Fig. 3(d, f)) also indicated the presence of these characteristic peaks, but with a decrease in the peak at 284.5 eV ($C\text{-sp}^3/C\text{-sp}^2$) and an increase in the relative area of the centered peak at 288.8 eV (COOH). These results indicate that the presence of nanomaterials in the membrane matrix decreases the content of C–C bonds at the expense of COO^- bonds, as expected due to the incorporation of oxygenated functions from GO and GO-SF. The high resolution spectrum of N1s for the pristine membrane hPAN (Fig. 3(c)) showed three peaks at 399.3 (73.7%), 400.1 (20.1 %) and 401.6 (6.2%) eV, referring to the bonds C–N/ $C\equiv N$, $C = N/(N-C = O)$ and $N-(C)_3$, respectively [55–57]. Pérez-Álvarez [54] when evaluating the optimization of the alkaline hydrolysis process of polyacrylonitrile membranes, observed that as the oxygen content increases on the membrane surface, there is a progressive decrease in the nitrogen in the composition. This trend is related to the hydrolysis mechanism, which although in a first stage maintains the N and O content constant, in a second stage the N content decreases while the O increases due to the loss of cyano groups for the formation of carboxylic groups [54]. For membranes with GO and GO-SF the deconvolution of N1s (Fig. 3(e,g)) showed the disappearance of the peak centered at 401.6 eV (tertiary amines), which ends up being masked due to the incorporation of COO^- bonds in the structure by the nanoadsorbents.

3.2.2.2. Morphological properties. The morphology of the surface and cross-section of the dry membranes was assessed by SEM analyses as shown in Fig. 4(a1–g1). All membranes presented a dense and thin upper layer with a finger-like sublayer. SEM images of the surface of the materials showed that the membranes of hPAN, hPAN@GO 2% and hPAN@GO-SF 2% had a dense and smooth upper layer; this morphological profile was modified with the increment of nanomaterial. The images indicated that the greater the content of GO and GO-SF in the membrane, the greater the presence of nanosheets on the surface of the material. The increase in nanomaterial content in the membrane also affected the morphology of the materials' cross-section. hPAN, among all other membranes, had a symmetric and thin finger-like sublayer which was altered according to the amount of incorporated GO and GO-SF. As nanomaterial content increased, the sublayer structures became asymmetrical and tended to thicken, decreasing the spacing between them. In membranes with higher content of GO and GO-SF, the finger-like structure was no longer observed, giving rise to a structure with compacted walls.

These conformations suggest that when added to the casting solution, nanomaterials create zones of high hydrophilicity in polymer membranes, due to the hydrophilic groups of GO and GO-SF nanosheets, which leads to an accelerated rate of water diffusion during the process of phase inversion, causing a rapid solidification of the membrane [58]. Dias et al. [59], when studying the influence of viscosity on the morphology of polyethersulfone hollow fiber membranes with additives, reached the same conclusion. According to the authors, the incorporation of nanomaterials increased the viscosity of the casting solutions, which in turn reduced the diffusion rate between the solvent and the non-solvent in the membrane sublayer, resulting in a quick surface demixing, triggering a densification in the upper layers and a slow internal precipitation. Regarding membrane thickness, no significant changes were observed, and the values varied between 260.8 and 279.4 μm . This indicates that although the casting solutions are more viscous, the presence of GO and GO-SF in the solution does not affect membrane thickness. These results were expected, since variations in the thickness of polymeric membranes with nanomaterials are only common in layer-by-layer assembly processes [27].

The AFM analyses were performed in liquid medium to assess the real characteristics of the membranes, since they are measured in water without going through the drying process that changes several parameters of membranes. Unlike the SEM technique presented above, AFM in liquid media makes it possible to assess the porosity and measure the

roughness of the new membranes within their actual testing conditions. After being synthesized, the hPAN, hPAN@GO and hPAN@GO-SF membranes are stored submerged in water and used without drying in the water purification. When wet, the membranes are soft to the touch, elastic and dense; once dry, they become rigid, fragile and brittle. The SEM analysis discussed above, therefore, describes the physical characteristics of membranes when dry, and may not match the actual morphological properties of the materials used in the tests. In turn, AFM in liquid medium, a technique that is rarely used in current studies, portrays with greater accuracy and precision the physical characteristics of membranes.

Thus, the surface morphology of wet membranes was assessed in AFM in liquid medium as shown in Fig. 4(a2–g2). The image of the hPAN membrane showed apparent pores on the upper surfaces and high surface roughness, with an estimated mean square roughness index (Sq) of 226.5 nm. These characteristics were reduced with the incorporation of GO and GO-SF in the membranes. When only 2% by mass of GO was added, the amount of apparent pores on the upper surface of the membrane became negligible and the Sq dropped to 14.9 nm. Furthermore, with the increase of 6% and 10% in mass of GO in the membrane, the Sq of the materials were estimated at 68.3 nm and 101.9 nm, respectively. No pores on the upper surface of these membranes were verified in the AFM images acquired in liquid media. This same morphological profile was observed for membranes containing GO-SF. With the increase in nanomaterial content of 2, 6 and 10%, there was progressive rise in the Sq of the materials, reaching 8.3, 17.1 and 39.2 nm, respectively. No pores on the upper surfaces of the membranes were verified either. The hPAN@GO-SF membrane less rough surface than hPAN@GO because the GO-SF is more hydrophilic than GO (Table 2).

Analyzing the results, it is clear that the addition of graphene nanomaterials to the membrane reduces pore size on the upper surfaces, which was not observed in the images. Also, the surface roughness of hPAN tends to increase according to the increment of material in the pristine membrane. These conformations indicate that the incorporation of GO and GO-SF in the casting solution, by creating zones of high hydrophilicity in the polymeric membranes, accelerates the process of external solidification of the membrane during the phase inversion process, generating an upper layer with narrow pores [26]. Furthermore, the increased roughness with the increment of materials in membranes may be related to the nucleation effect of GO and GO-SF nanosheets; the presence of these nanomaterials on the surface of the membranes increases compound crystallization leading to the formation of large crystal grains in the structure [60]. Similar results were observed by Zhu et al. [61] when preparing PVDF nanohybrid membranes with GO. According to the authors, the absence of apparent pores on the upper surfaces of the membranes was related to the preparation of the material. When the molding solution containing the polymer and the GO was submerged in water, the outer surface of the membrane instantly solidified, generating a thin and dense layer. The difference in roughness of membranes with different contents of GO was attributed to the nucleation and growth of the polymer induced by the addition of the nanomaterial. According to the authors, when using a smaller amount of GO (0.5% by weight) in the casting solution, there could be an induction of more nuclei and smaller crystal grains leading to the formation of a less rough upper surface, increasing according to the increment of nanomaterial.

The dry membranes were also analyzed through X-ray computed microtomography (Micro-CT) to obtain more information about the structure and porosity of the membranes. The relevant descriptions of the porosity of membranes (10x10 mm) as well as the images obtained are shown in Table 1 and Fig. 4(a3–g3), respectively. It can be observed that the hPAN membrane has the lowest volume of interest (VOI) (3.1 m^3) and the variation in nanomaterial content increased the VOI to 3.5 and 3.6 m^3 in the case of hPAN-GO 10% and hPAN-GO-SF 10%, respectively (Table 1). Regarding the porosity rate, the same behavior was observed. The pristine membrane had a lower average porosity of

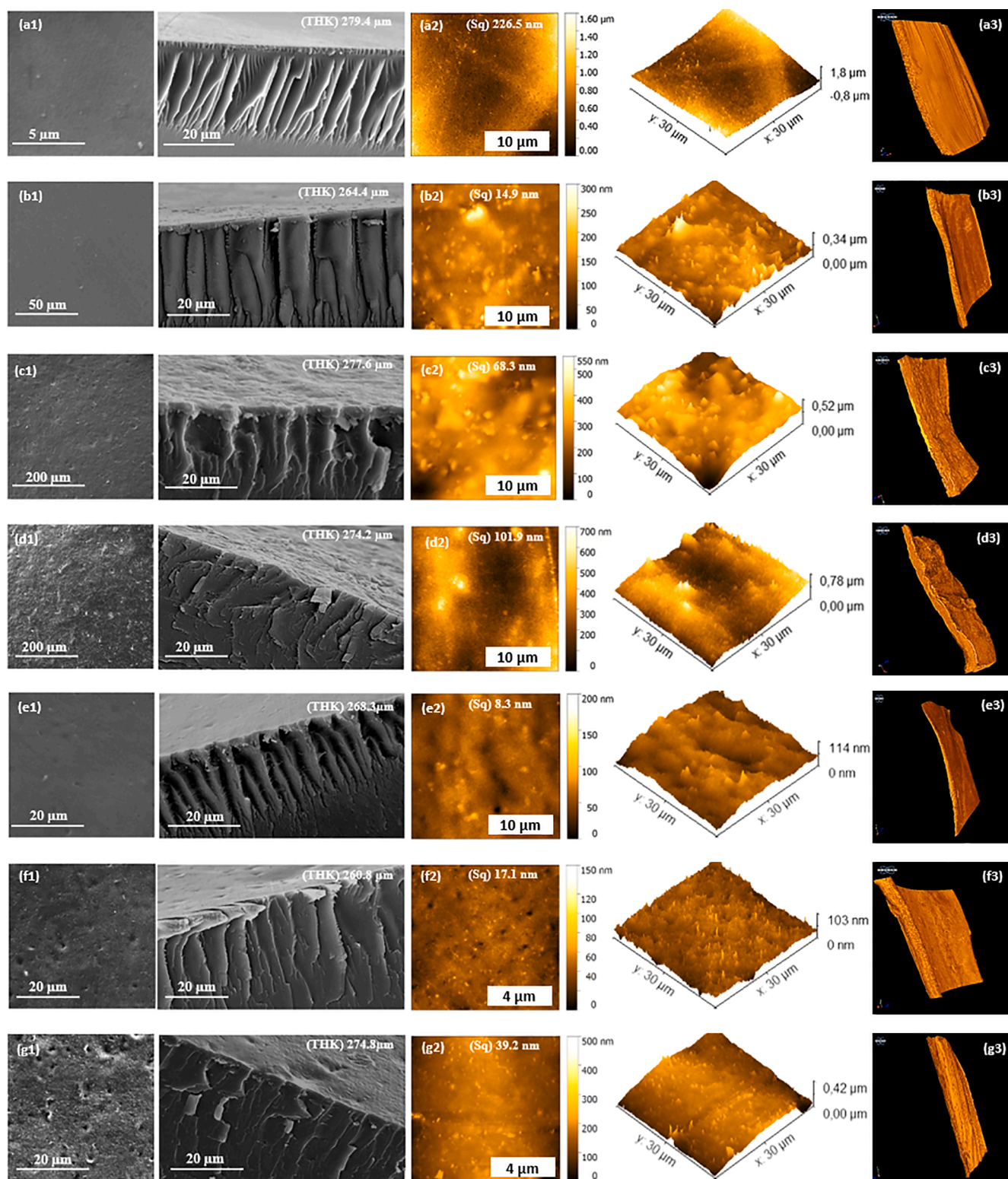


Fig. 4. SEM images of the surfaces and cross sections of (a1) hPAN; (b1) hPAN@GO 2%; (c1) hPAN@GO 6%; (d1) hPAN@GO 10%; (e1) hPAN@GO-SF 2%; (f1) hPAN@GO-SF 6%; (g1) hPAN@GO-SF 10% membrane; AFM images in liquid media of (a2) hPAN; (b2) hPAN@GO 2%; (c2) hPAN@GO 6%; (d2) hPAN@GO 10%; (e2) hPAN@GO-SF 2%; (f2) hPAN@GO-SF 6%; (g2) hPAN@GO-SF 10% membranes. Micro-CT images of (a3) hPAN; (b3) hPAN@GO 2%; (c3) hPAN@GO 6%; (d3) hPAN@GO 10%; (e3) hPAN@GO-SF 2%; (f3) hPAN@GO-SF 6%; (g3) hPAN@GO-SF 10% membranes. Where THK is the thickness membrane and Sq is root mean square roughness membrane.

Table 1

Brief description of the porosity of membrane samples by micro computed tomography.

Material	MicroCT Analyses Data		
	Total VOI volume (m ³)	Volume of pores (m ³)	Porosity (%)
hPAN	3.08	2.75	89.29
hPAN@GO 2%	3.08	2.82	91.48
hPAN@GO 6%	3.30	3.10	91.63
hPAN@GO 10 %	3.54	3.23	93.84
hPAN@GO-SF 2%	3.09	2.80	89.55
hPAN@GO-SF 6%	3.41	3.05	90.04
hPAN@GO-SF 10%	3.61	3.25	90.67

89.3%, and it increased according to the nanomaterial content, reaching maximum values of 93.9 and 90.7 % for the hPAN-GO 10% and hPAN-GO-SF 10% membranes, respectively. Therefore, the addition of GO and GO-SF changed the polymer casting solution viscosity, although it accelerated the surface demixing rate of the new membranes, generating denser upper layers. It also reduced the diffusion rate between the solvent and non-solvent in the sublayer of materials, leading to formations of thicker and asymmetrical finger-like structures in the sublayers of membranes with higher nanomaterial content. This modification in the internal structure of the materials, according to MicroCT, increases the average porosity of the materials and consequently the VOI. Similar results were obtained by Otitoju et al. [62] in the preparation of nanocomposite membranes endowed with different nanoparticles (NPs). On average, the porosity of composite membranes (78–80%) was higher than that of the pristine membrane (70%). According to the authors, porosity can be influenced by the casting solution and the hydrophilicity

effect of inorganic NPs. The presence of different compounds resulted in a faster phase inversion, increasing the exchange rate between non-solvent and solvent in the membrane, thus resulting in increased pore formation in the material.











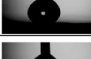
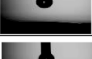






















3.2.2.3. Water contact angle. The hydrophilicity of the surface of prepared membranes was determined by the measurements of the water contact angle, and the detailed variation of this parameter over time is described in Table 2. A hydrophilic surface exhibits a static contact angle with water of less than 90°, while a hydrophobic surface exhibits a static contact angle above 90° [63]. Thus, analyzing the results for the membranes (3.6°–32.1°) it was possible to conclude that all of them have a good wetting surface, being hydrophilic in nature. This characteristic influences the minimization of permanent adhesion of scale on the membrane surface and increases water flux [64].

Although all analyzed membranes have a hydrophilic surface, the values observed between them diverge. A remarkable change in the contact angle between PAN and hPAN was observed, decreasing from 32.1° to 3.7°, respectively. This discrepancy was associated with membrane hydrolysis. The PAN membrane has repetitive hydrocarbon and CN groups in its structure, making it less hydrophilic in nature [65], which results in the largest observed contact angle. During the alkaline hydrolysis of PAN membranes, carboxyl groups and amides are formed in the polymer matrix, which increases the hydrophilicity of the membrane [53], culminating in the reduction of the contact angle with water.

Regarding membranes containing nanomaterials, an increase in the water contact angle was observed with the increment of GO and GO-SF dosage in the membranes, ranging from 3.5° to 17.6° and 3.6° to 6.9°, respectively. In the case of hPAN@GO, GO is formed by a domain of hydrophobic carbons hybridized in sp² in the basal plane which is bound to hydrophilic carboxyl, hydroxyl, epoxy and carbonyl groups on the edges of the nanosheets [66], having hydrophobic and hydrophilic

Table 2

The water contact angle for PAN, hPAN, hPAN-GO and hPAN@GO-SF with different nanomaterials content.

	DWCA (θ°) at 10 second	Images of the contact angle at different intervals		
		0,1s	3s	10s
		PAN	32.07	
hPAN	3.65			
hPAN@GO 2%	3.53			
hPAN@GO 4%	4.28			
hPAN@GO 6%	5.91			
hPAN@GO 8%	8.37			
hPAN@GO 10%	17.63			
hPAN@GO-SF 2%	3.63			
hPAN@GO-SF 4%	4.32			
hPAN@GO-SF 6%	5.41			
hPAN@GO-SF 8%	6.43			
hPAN@GO-SF 10%	6.95			

domains. Thus, when incorporated into hPAN, GO contributes to decreasing the hydrophilicity of the membranes, reaching 17.3° of water contact angle. In relation to hPAN@GO-SF membranes, the insertion of GO-SF also enhanced hydrophobicity, though to a lesser extent, reaching the maximum value of 6.9° . This is probably due to the incorporation of SF dye, which contains two amino and one phenazinium salt in its structure, providing more hydrophilicity to the membrane when compared to GO [67].

3.2.2.4. Pure water flux (PWF). Filtration assays with pristine and nanomaterials-incorporated membranes were carried out to evaluate pure water flux (PWF) (Fig. 5). Pristine hPAN, hPAN@GO 2% and hPAN@GO-SF 2% showed higher PWF, reaching 185.8, 183.1 and 180.5 $\text{L}\cdot\text{m}^{-2}\cdot\text{h}^{-1}$, respectively. The hPAN@GO 6% and hPAN@GO-SF 6% membranes showed intermediate PWF values of 137.9 and 127.4 $\text{L}\cdot\text{m}^{-2}\cdot\text{h}^{-1}$, respectively. While lower values were obtained for the membranes with 10% of nanomaterial, with hPAN@GO-SF 10% ($87.6 \text{ L}\cdot\text{m}^{-2}\cdot\text{h}^{-1}$) outperforming than hPAN@GO 10% ($39.8 \text{ L}\cdot\text{m}^{-2}\cdot\text{h}^{-1}$). This behavior of water flow reduction with the increment of nanomaterial in the membrane is associated with factors such as hydrophilicity and porosity of the membranes.

The higher flux presented by hPAN, hPAN@GO 2% and hPAN@GO-SF 2% can be attributed to the slightly superior hydrophilic character of these membranes when compared to the others containing higher nanomaterial content (Table 2). Greater hydrophilicity increases the attraction of water molecules and the membrane matrix, resulting in higher PWF values [60]. Regarding the higher PWF of hPAN, the presence of pores in the outer layer of material, not visible in the membranes with GO and GO-SF (Fig. 4(a1-g1)), suggests increased pore size in the superficial layers of the pristine membrane, and large pores result in greater water permeation [28]. In the case of membranes incorporated with higher nanoadsorbent content, the decrease in hydrophilicity of the materials with the increase of GO and GO-SF (Table 2) culminated in reduced attraction of water molecules into the interior of the polymer matrix. Being hPAN@GO-SF 10% more hydrophilic than hPAN@GO 10% (Table 2), the obtained results were expected. Besides hydrophilicity, the fact that the GO membrane has an internal finger-like structure more asymmetric and less spaced than the GO-SF membrane (Fig. 4(a-g)) indicates greater blockages of the internal connections between the pores of the materials, which contributes to a decrease in the water flux. Beluci et al. [68] observed a similar behavior when evaluating the PWF of a biopolymer incorporated with GO. The pure membrane showed higher PWF ($230 \text{ L}\cdot\text{m}^{-2}\cdot\text{h}^{-1}$) compared to the modified

membranes ($120 - 0.3 \text{ L}\cdot\text{m}^{-2}\cdot\text{h}^{-1}$). In addition to the hydrophilicity of the membranes, which decreased with the increase of GO in the material, the authors related this conformation to the nanoadsorbent accumulation in the polymeric matrix, which obstructed the membrane pores and made it difficult for water to pass through.

3.2.2.5. Zeta potential. The zeta potential measurements of PAN and hPAN, as well as of hPAN@GO and hPAN@GO-SF membranes in the pH range 4–10 are shown in Fig. 6. The PAN membrane (Fig. 6a) showed an electronegative potential (-11.17 to -16.65 mV) mainly due to the ionization of nitrile groups ($\text{C}\equiv\text{N}$) of PAN in response to pH change [69]. When PAN is hydrolyzed in alkaline solution, the surface charge of the hPAN membrane becomes more negative (-15.20 to -34.95 mV). The alkaline hydrolysis of the PAN membrane generates carboxyl and amide groups in the membrane matrix, conferring a greater negative character and better selectivity in the adsorption of organic compounds [53].

hPAN@GO and hPAN@GO-SF membranes (Fig. 6(b,c)) showed a rise in zeta potential with the increase in nanomaterial content in the membrane. hPAN@GO membranes (2–10 wt%) showed greater negative potential (-20.30 to -44.53 mV) than hPAN@GO-SF membranes (2–10 wt%) (-15.63 to -40.8 mV). GO has several carboxyl, hydroxyl, epoxy and carbonyl groups in the basal plane and edges of the sheets, which contributes to its electronegative character [70]. Thus, when incorporated into hPAN membrane, GO enhanced the negative charge on the surface of the new material. In relation to hPAN@GO-SF, the GO-SF surface is less electronegative due to the insertion of the cationic dye safranin into the GO matrix. Thus despite the contribution of oxygenated groups to GO, the insertion of phenazinium cation of SF [71] into the GO surface reduces the negative charge of the membrane. Therefore, the incorporation of GO-SF into the hPAN membrane afforded a lower negative surface charge compared to hPAN@GO membranes. Furthermore, it is possible to observe that up to 4% increase in GO-SF mass, the new membrane had a lower electronegative potential than hPAN, unlike what was observed with hPAN@GO membranes, confirming the presence of safranin dye attached on GO.

3.3. Adsorption studies

The new prepared membranes were submitted to adsorption of ECs in batch and continuous flow processes. The purpose of this part of the work was to evaluate the potential of these membranes as adsorbent and filtering agents, as well as to understand how the presence of GO and GO-SF could influence the membranes' adsorptive potential. To this end,

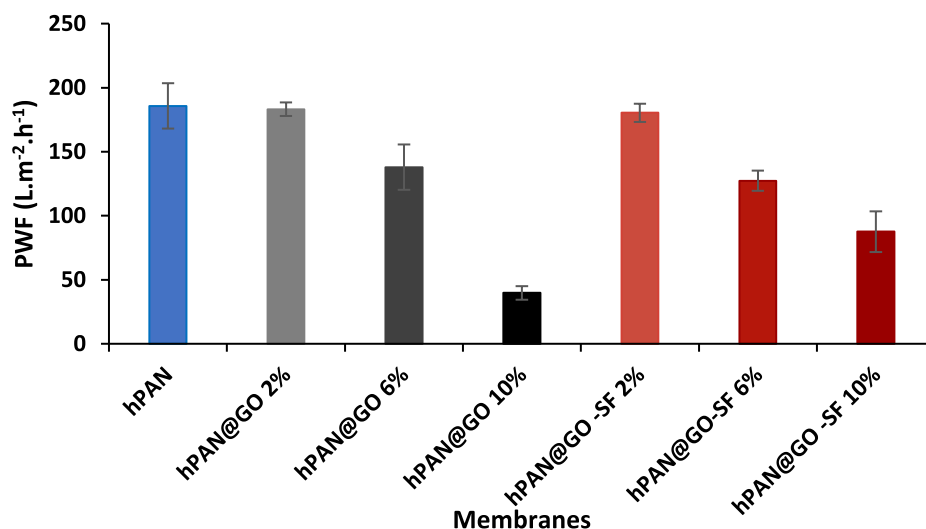


Fig. 5. (a) PWF of hPAN (blue blocks), hPAN@GO (black blocks) and hPAN@GO-SF (red blocks) membranes. 5 cm average membrane diameter, 1 bar of pressure, pH 6 and at room temperature.

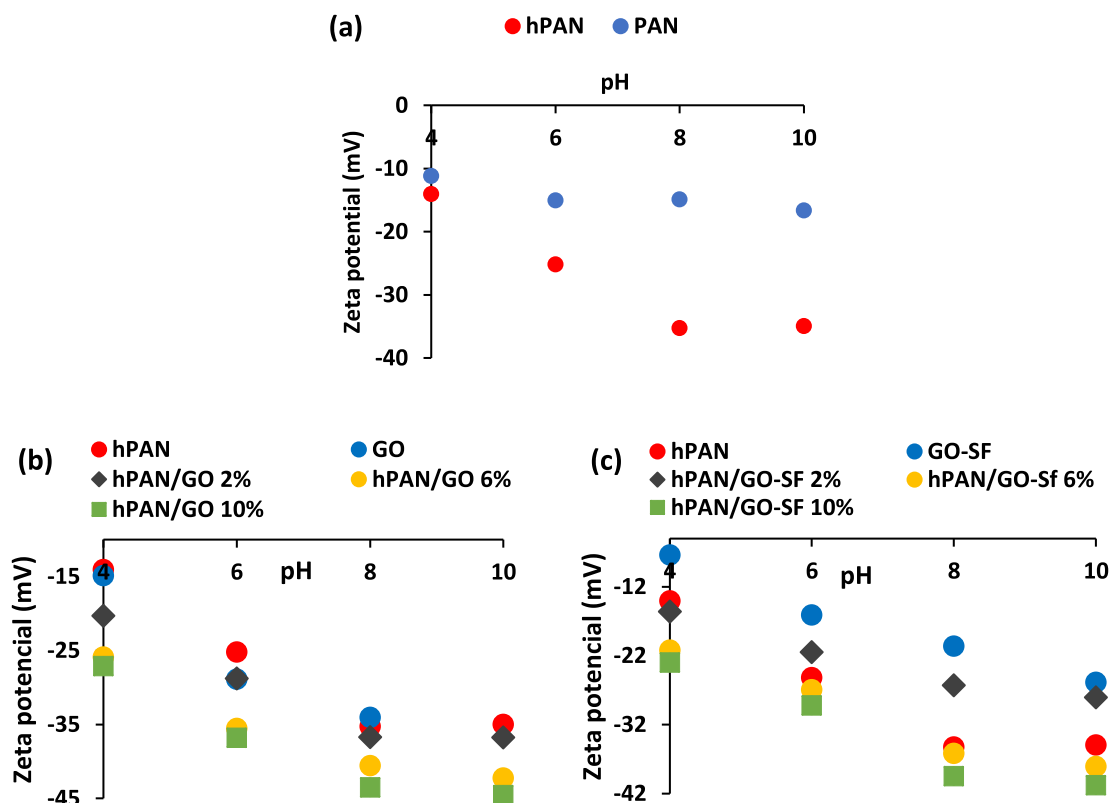


Fig. 6. Zeta potential measurements of (a) hPAN (blue circle) and PAN (red circle), (b) hPAN@GO membranes with different GO content and (c) hPAN@GO-SF membranes with different GO-SF content.

hPAN, hPAN@GO 6% and hPAN@GO-SF 6% membranes were used. The separation of charged solutes from permeation by filter membranes mainly involves parameters such as steric hindrance and electrostatic adsorbent/adsorbate interactions [72]. As reported in the literature, porous membranes with more retained sublayers, with intermediate fluxes (above $90 \text{ L}\cdot\text{m}^{-2}\cdot\text{h}^{-1}$) and electrostatic potentials, outperform others in removing charged contaminants [68]. In this regard, membranes incorporated with nanomaterials at 6% were selected. These membranes, with finger-like narrower macrovoids and upper intermediate roughness, due to steric hindrance, presented greater potential for the retention of contaminants. In addition, the good permeance of the membranes and their electronegative potential helped in the interactions of the solute in the material.

3.3.1. Batch adsorption study

The adsorption potential of membranes in batch assays for common ECs was evaluated for the anionic dyes remazol brilliant blue (RRB), reactive orange 122 (OR122), direct black 22 (BB22) and acid black 194 (AB194); the cationic dyes basic brown 4 (BB4), methylene blue (MB) and basic Blue 7 (BB7); the surfactants benzalkonium chloride (BZC) and cetylpyridinium chloride (CPC); and the pharmaceutical drug propranolol (PRO). The use of membranes in batch adsorption experiments has the great advantage of the easy removal of the adsorbent from the aqueous medium post-process, eliminating the filtration step that makes the purification process more expensive.

The results obtained, subdivided in anionic dyes and cationic contaminants, are shown in Fig. 7(a,b). The overall results showed that for different classes of contaminants, the composite membranes hPAN@GO and hPAN@GO-SF had higher adsorption capacity compared to pristine hPAN membranes, indicating that the incorporation of graphene nanomaterials into hPAN membranes enhanced their adsorbent performance.

The results obtained in anionic dyes adsorption (Fig. 7(a)) indicated that hPAN@GO-SF membranes had higher adsorption capacity than

hPAN@GO membranes, with potentials of 39.9 versus $14.9 \text{ mg}\cdot\text{g}^{-1}$ for RBB, 28.4 versus $26.1 \text{ mg}\cdot\text{g}^{-1}$ for RO122, 29.1 versus $10.6 \text{ mg}\cdot\text{g}^{-1}$ for DB22 and 11.6 versus $3.9 \text{ mg}\cdot\text{g}^{-1}$ for AB194, respectively. The results suggest that the adsorption process of anionic dyes occurs mainly by electrostatic interactions. GO and GO-SF provided oxygenated and phenolic groups to the membranes, which may have improved their adsorbent ability enabling π - π interactions between adsorbent/adsorbate [28]. The hPAN@GO membranes, which had higher electronegativity zeta potential (Fig. 6), showed lower adsorption capacities than the hPAN@GO-SF membranes, probably due to electrostatic repulsion with anionic dyes. In turn, the hPAN@GO-SF membrane have a less charged surface compared to hPAN@GO, due to the incorporation of phenazinium cations into the structure, which may have generated less electronegative surface zones on the membrane. These domains enabled greater proximity between the anionic dye and the membranes through electrostatic attractions, and these adsorbent/adsorbate interactions, in turn, favored other interactions, such as hydrogen bonding and π - π .

When cationic ECs were used in the adsorption tests, excellent results were observed (Fig. 7(b)). The hPAN@GO-SF membranes outperformed the hPAN@GO membranes with maximum adsorption potentials estimated at 200.6 versus $177.4 \text{ mg}\cdot\text{g}^{-1}$ for the pharmaceutical PRO, 154.8 versus $129.3 \text{ mg}\cdot\text{g}^{-1}$ for BZC surfactant and 191.1 versus $183.5 \text{ mg}\cdot\text{g}^{-1}$ for MB dye, respectively. Suggesting that the adsorption process of these contaminants by membranes, in addition to taking place via electrostatic and π - π interactions, has an influence on the physical and mechanical properties of the membrane. Regarding the interactive processes by physicochemical bias, while hPAN mostly governs the adsorption of organic contaminants via electrostatic interactions and hydrogen bonding [73], the presence of GO-derivatives in both materials, as previously commented, would enable π - π interactions between adsorbent/adsorbate [74]. On the other hand, the presence of SF in the material could cause electrostatic repulsions between hPAN@GO-SF and cationic contaminants, thus reducing the adsorption potential of the

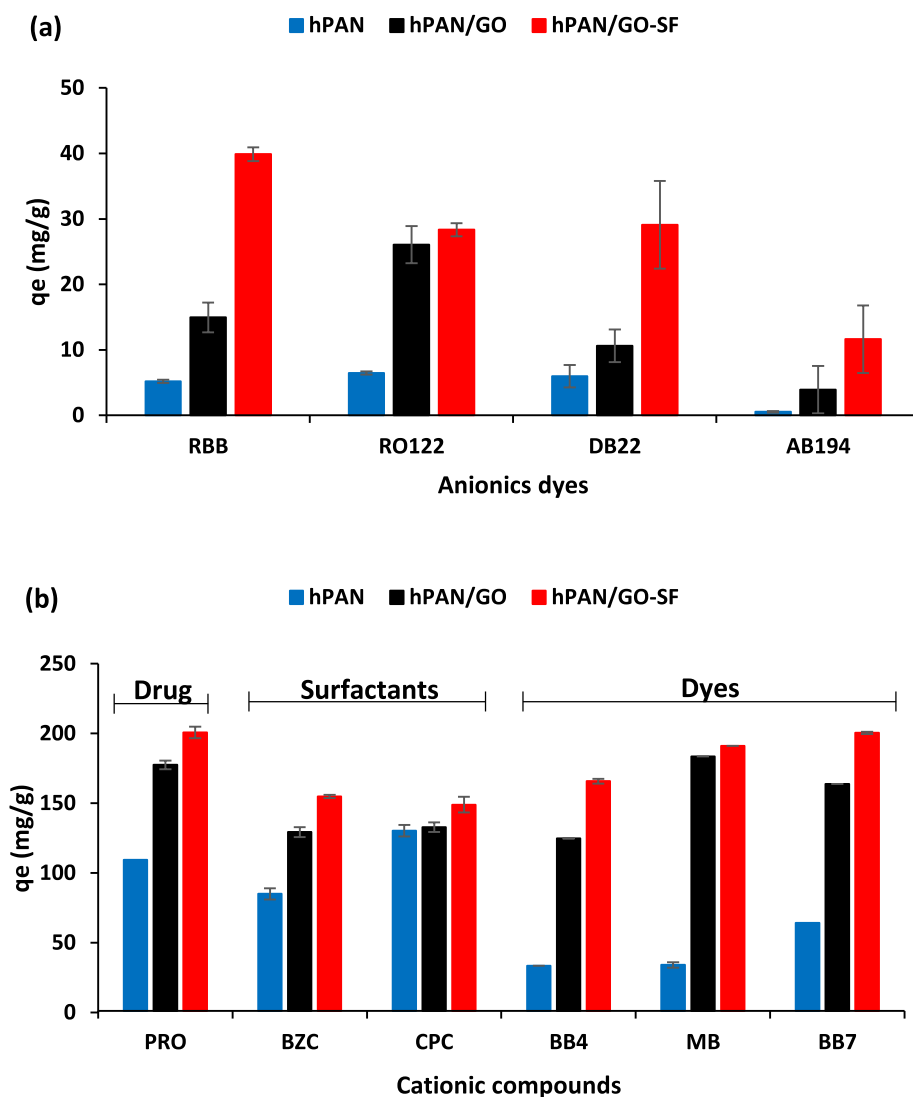


Fig. 7. Batch adsorption of (a) Cationic contaminants by hPAN (blue blocks), hPAN@GO (black blocks) and hPAN@GO-SF 6 (red blocks) membranes and (b) Anionic contaminants by hPAN (blue blocks), hPAN@GO (black blocks) and hPAN@GO-SF (red blocks) membranes. Nanomaterial dosage of membranes 6%, membrane amount 0.01 mg, volume of 5 mL, initial concentration of contaminants $100 \text{ mg}\cdot\text{L}^{-1}$, agitation of 180 oscillations/min, pH 6 and at room temperature.

membrane. However, the results obtained indicated the opposite, corroborating to the zeta analysis (Fig. 6), which indicated that the hPAN@GO-SF membranes still had a negative surface charge, despite the cationic dye incorporation. This suggests that, like hPAN@GO membranes, hPAN@GO-SF membranes interact with cationic compounds through electrostatic, π - π and hydrogen bonding interactions.

Therefore, considering that both membranes, hPAN@GO and hPAN@GO-SF, interact in a similar physicochemical way with cationic compounds, what might contribute to hPAN@GO-SF membranes excelling in the removal of this class of compounds? According to the performed characterizations, hPAN@GO-SF has different mechanical properties than hPAN@GO, suggesting that changes in the material structure influence its removal potential. Few studies in the literature related the morphology surface of polymeric membranes to its potential to removal organic compounds in batch adsorption process [75]. However, studies involving the adsorption of organic compounds on carbonaceous [76] and silica [77] surfaces have already reported the influence of substrate roughness on the adsorbent/adsorbate interactive process. According to these works, the rate of activation energy required for the adsorption of compounds increases with the roughness of the substrate, making adsorption difficult. The higher the surface roughness of the material, the lower its adsorption potential. In an analogous way,

the new hPAN@GO-SF membranes for having a less rough and porous surface, when compared to hPAN@GO and hPAN, contribute to a better adhesion of contaminants on the polymer matrix. In turn, this adsorbent/adsorbate proximity contributes to greater physicochemical interactions between membrane and organic compounds.

3.3.1.1. DFT-based molecular chemical descriptors calculations and batch assays. DFT calculations were carried out to achieve a deep understanding of the reactivity of organic compounds in the interactive adsorbent/adsorbate processes with emphasis on the molecular and electronic properties of adsorbates. For the DFT calculations, we selected one cationic contaminant from each class that stood out in the membrane adsorption process due to high adsorption capacities. Thus, BZC was the surfactant, MB was the dye and PRO was the drug. The geometric optimization of the isolated compounds used the B3LYP method and the molecules were evaluated by the molecular basis 6-31G (d, p), which among those analyzed had the lowest energy and therefore more stable structures.

Fig. 8(a-c) shows the optimized molecular structures of BZC, MB and PRO, and the size of the molecules, which were estimated at 22.9 Å, 14.2 Å and 14.3 Å, respectively. While the optimized structures of the drug and dye exhibited molecules with planar tendencies due to the

π -conjugate system, the surfactant had a twisted long carbon chain due to hysterical carbon repulsion. The conformation of contaminant molecules, as well as their size, are fundamental parameters for evaluating the interactions of these compounds with solid surfaces. Large, twisted molecules make it difficult for the compound to contact the sites of interaction of solids, due to steric hindrance, as demonstrated by Deepatana et al. [78].

Fig. 8(d-f) shows the 3-D contours of the HOMO (E_H) and LUMO (E_L) molecular boundary orbitals of the compounds BZC, MB and PRO. Considered the main orbitals in the chemical stability of molecules, E_H represents the highest energy occupied orbital, with potential to donate electrons, while E_L represents the lowest energy empty orbital, with potential to receive electrons [79]. Thus, E_H energy is linked to reactivity to the electrophilic attack of the compounds and E_L energy to reactivity to the nucleophilic attack [80]. Of the compounds, MB has a greater tendency to donate electrons ($HOMO \gg$) and to accept electrons ($LUMO \ll$). The E_H - E_L energy gap (Δ_{H-L}) (Fig. 8(d-f) and Table 3), molecular conformation barrier, provides information regarding the stability and reactivity of the compounds. The higher the Δ_{H-L} , the greater the stability of the molecule and, consequently, the lower its reactivity towards the adsorbent and vice versa. MB has a lower Δ_{H-L} (0.04238 eV) compared with BZC (0.12368 eV) and PRO (0.17068 eV), suggesting that MB has greater reactivity towards the adsorbent.

Regarding the other molecular chemical descriptors described in Table 3, chemical potential (μ), global chemical hardness (η) and electrophilicity index (ω) also corroborate the previous statement. Electronic chemical potential (μ), responsible for determining the tendency of electrons to leave the system [81] and global chemical hardness (η), a parameter that provides information about the resistance to deformation in the electron density of a molecule [82], are key indicators of a molecule's general reactivity and essential descriptors in determining charge transfer during a chemical interaction [80]. The most reactive molecule is characterized by high μ and low η values. MB, PRO and BZC

Table 3

Obtained data for molecular chemical descriptors, HOMO and LUMO energy for BZC, MB and PRO.

Molecular Chemical Descriptors	BZC	MB	PRO
Experimental q_e (mmol.g^{-1})	0.4964	0.5975	0.7742
HOMO energy (E_H , eV)	-0.17169	-0.16069	-0.19819
LUMO energy (E_L , eV)	-0.04801	-0.11831	-0.02751
Energy gap (Δ_{H-L} , eV)	0.12368	0.04238	0.17068
Chemical Potential (μ , eV)	0.10985	0.13950	0.11285
Chemical hardness (η , eV)	0.06184	0.02119	0.08534
Electrophilicity index (ω , eV)	0.09757	0.45918	0.07461

have μ of 0.13950 eV, 0.11285 eV and 0.10985 eV, respectively, and estimated η of 0.02119 eV, 0.08534 eV and 0.06184 eV, respectively, indicating that MB is the most reactive among the molecules analyzed. When indicating the stabilization of the system saturated by electrons ω gives information about structural patterns, selectivity and reactivity of molecules [83]. A higher ω indicates that the compound has a tendency to accept electrons until the molecule's energetic stabilization. Lower values were obtained for the BZC and PRO molecules, 0.09757 eV and 0.07461 eV, respectively, indicating that these compounds are less reactive than MB.

Considering the adsorption potential of hPAN@GO-SF membranes towards the molecules of the contaminants, it was observed that the modeling data showed some discrepancies in relation to the affinity tests. As seen in Table 3, experimental results showed that PRO was the most removed contaminant (0.8 mmol.g^{-1}), followed by MB (0.6 mmol.g^{-1}) and BZC (0.5 mmol.g^{-1}). According to the DFT study, the dye molecule, due to its greater reactivity and greater propensity to undergo electron density deformations, should have been most adsorbed contaminant by the membrane, followed by BZC and PRO molecules, respectively. The DFT calculations, when investigating the electronic structure of organic molecules, mainly provides clues about π - π

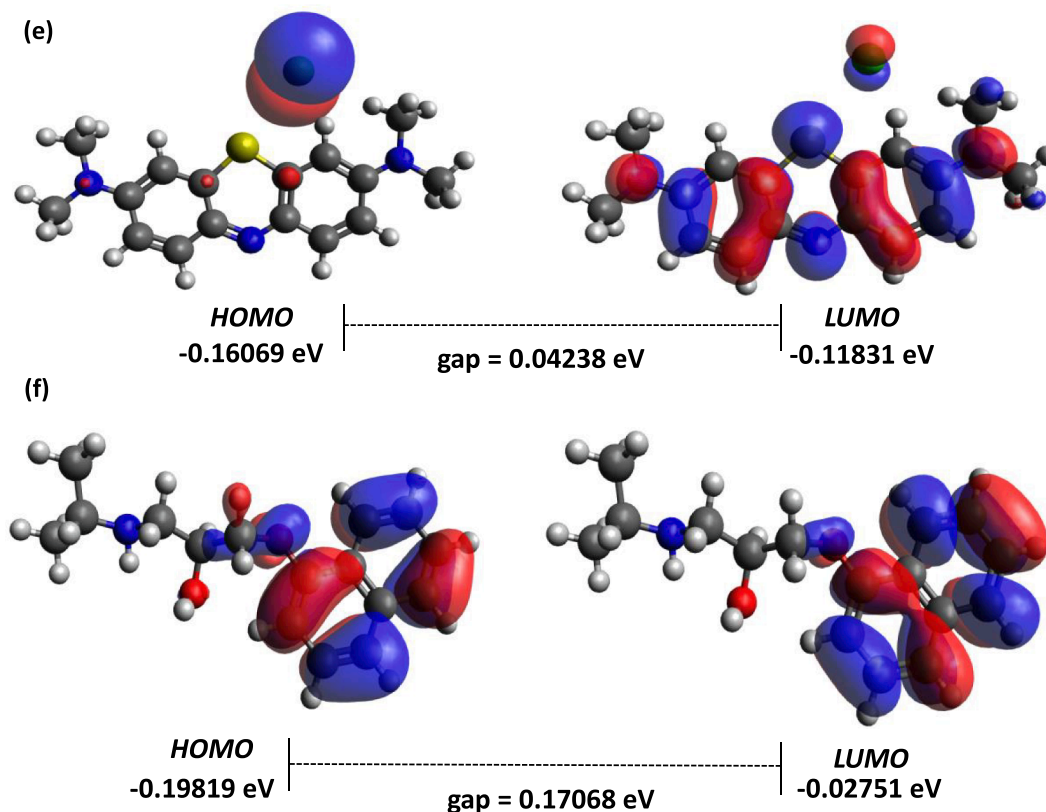


Fig. 8. Optimized structures size of (a) BZC; (b) MB; (c) PRO. Tridimensional frontiers orbitals HOMO and LUMO plots of (d) BZC; (e) MB; (f) PRO (blue color: positive phase; red color: negative phase).

interactions [84]. Therefore, the results obtained suggest that the MB/membrane system has a greater contribution of π - π interactions than the PRO and BZC systems.

The analyzed molecules have cations in their structures and since the membranes are electronegative, electrostatic interactions are possible, which are not considered in the DFT calculations performed [85]. Furthermore, PRO endowed with NH and OH groups can interact with the COO^- of the membranes by hydrogen bonding [86]. Thus, to assess how much these other interactions are present in the adsorptive process, tests in saline medium were performed (Fig. S2). In this system, the excess of Na^+ and Cl^- ions competing for the material's interactive sites is indicative of possible electrostatic and hydrogen bond adsorbent/adsorbate interactions [87]. The decrease in the adsorption capacity of hPAN@GO-SF for the contaminants indicated that about 82% (Fig. S2) of PRO interactions are related to electrostatic and hydrogen interactions, while for BZC and MB that figure is about 69 and 62% (Fig. S2), respectively. These results confirm that, in addition to π - π interactions, the adsorptive process of membranes includes electrostatic and hydrogen bonds.

Thus, the conjuncture of the results suggests that PRO, when interacting with the membrane through hydrogen bonds and π - π and electrostatic interactions, is better adsorbed by the material, and MB and BZC, given the π - π and electrostatic bonds, are respectively the second and third compounds better adsorbed by hPAN@GO-SF. In the case of BZC, in addition to the chemical bias, the decrease in its adsorption potential is related to the steric impediment of the compound, which, due to the formation of micelles, has a large structure [38].

3.3.1.2. Post adsorption XPS analysis. XPS analysis of post-adsorption in batch assays of hPAN@GO-SF 6% membrane was performed to evaluate the adsorbent/adsorbate interactions according to variations in the elemental composition and chemical bonds of the materials (Fig. 9(a-g)). Regarding the XPS survey spectrum, the hPAN@GO-SF membrane before adsorption endowed with C, O, N, Na and Cl in a content of 76.4, 10.3, 12.5, 0.1 and 0.7 % (Fig. 3(a)), respectively. In the hPAN@GO-SF with BZC-loaded (Fig. 9(a)) the presence of surfactant in the membrane could be confirmed by the increase in C content (78.0%), and decrease in O (9.3%), Na (0%) and Cl (0.1%) contents. As the pollutant molecule was endowed with many carbons and does not have any oxygen (Fig. 8(a)), the increase of carbon and decrease of oxygen in the membrane was expected. Regarding the reduction of Cl and Na, this perspective suggests a cation exchange between the cationic BZC and Na^+ of hPAN@GO-SF [87]. In hPAN@GO-SF MB-loaded (Fig. 9(a)) there was an increase in N content (from 12.5 to 13.6%) and a disappearance of Cl and Na. The dye molecule endowed with nitrogen functional groups (Fig. 8(b)), so the increase of this element in the membrane was expected and the reduction of Cl, being the counter ion of MB dye, suggests the cation exchange between Na^+ of the membrane and the cationic dye [87]. Furthermore, the adsorption of MB to the membrane can also be attested due to the appearance of S (1.2%) in the sample, an element presents in MB dye (Fig. 8(b)). Regarding hPAN@GO-SF with PRO-loaded, the increase in O (10.8%) and N (12.9%), as well as the absence of Cl, attest to the adsorption of the contaminant to the material. As the PRO drug contains oxygenated and nitrogenous functional groups (Fig. 8(c)), an increase of these elements was expected. As above mentioned for the adsorption of BZC and MB, the disappearance of Cl and Na after the process indicates cation exchange of Na^+ and the cationic drug [88,89].

The C1s and N1s high resolution analyses of the membranes after the adsorptive process (Fig. 9(b-g)) indicated changes in binding energy and peak intensity of the materials compared to the pristine hPAN@GO-SF 6%, suggesting interactions between the material and the contaminating molecules [87,90]. The C1s high resolution XPS spectrum of the pristine membrane (Fig. 3(f)) indicated peaks at 284.2, 285.1, 286.1, 287.1 and 288.0 eV referring to the C = C/C-H, C-N/C-O, C-O-C, C = O,

COOH bonds, respectively. Shifts in binding energy attributed to C = C were verified, from 284.2 eV to 284.6, 284.7 and 284.4 eV for membranes containing BZC, MB and PRO (Fig. 9(b,d,f)), respectively. These results indicate the presence of π - π interactions between the aromatic rings of hPAN/GO-SF and contaminant molecules [90,91]. Moreover, the appearance of the peak at 291.4 eV in the membrane with PRO, referring to specific π - π interactions [92], which attests the presence of stronger interactions between the membrane and pharmaceutical drug, compared to BZC and MB. This perspective may be related to the electronic of the molecule, which has an electron-rich naphthalene ring that may be more reactive towards GO-SF adsorbent (Fig. 8(c))[93]. Shifting in peaks associated to C-O/C-N bonds from 286.1 eV to 286.0, 285.6 and 285.9 eV were also observed for membrane with BZC, MB and PRO adsorbed (Fig. 9(b,d,f)), respectively, indicating the presence of hydrogen bonds between adsorbent/adsorbate [94]. This could also be confirmed by shifting in energies related to the C = O interactions, which changed from 287.1 eV to 286.9, 287.6 and 287.8 eV for the membranes containing the contaminants BZC, MB and PRO (Fig. 9(b,d,f)), respectively [94].

The N1s deconvolutions of the hPAN@GO-SF 6% membrane before adsorption (Fig. 3(a)) showed peaks at 399.2 and 400.0 eV, referring to the C-N/C \equiv N and C = N/N-C = O bonds, respectively. For the membrane with BZC-loaded (Fig. 9(c)) these peaks shifted to 399.4 and 400.7 eV, respectively and for PRO (Fig. 9(g)), these were estimated at 399.4 and 400.5 eV, respectively. Regarding the hPAN@GO-SF adsorbed with MB (Fig. 9(e)), a single peak referring to the C = N/N-C = O bonds was observed at 399.4 eV. These shifting in binding energies suggest that nitrogen groups play important role in the adsorption mechanism, mainly in hydrogen bonds [57,95].

3.3.2. Continuous flow adsorption study

Considering that in the batch tests the new membranes showed a greater adsorption for cationic contaminants, filtration tests were performed only for this class of contaminant. The cationic dyes gentian violet (GV), basic blue 26 (BB26), basic green 4 (BG4), rhodamine B (RhB), MB and BB4 were available and the solute rejection by membranes are shown in Fig. 10. As in the batch tests, the general results showed that the composite membranes, hPAN@GO and hPAN@GO-SF, presented greater adsorption capacity compared to the hPAN membranes. Greater differences were found for the BB26, GV and MB dyes, where the pristine membrane reached values of 47.6, 39.9 and 27.3%, respectively. GO and GO-SF membranes reached superior rejection rates of 72.0% and 83.6% for BB26; 57.9% and 71.6% for GV; and 44.6% and 67.0% for MB, respectively. These results corroborate the data presented for PWF membranes (Fig. 5), which suggest that hPAN membranes, because of their larger surface pore sizes, have lower resistance to the retention of contaminant molecules. This reinforces once again that the incorporation of GO and GO-SF nanomaterials in pristine membranes, by generating greater blockages of the internal connections between the pores of the materials, potentiates their adsorbent character.

As mentioned above, hPAN@GO-SF membranes performed better than hPAN-GO. The highest rejection rates were found for the BB26 (83.6% versus 72.0%) and BG4 (90.6% versus 82.2%) dyes by hPAN@GO-SF and hPAN@GO, respectively. These results can be related to the roughness profile of the membranes. hPAN@GO-SF membranes, as they present lower mean square roughness than hPAN@GO membranes, tend to a greater imprisonment of dye molecules on their surface during filtration [96]. This longer contact time between adsorbent/adsorbate contributes to the establishment of chemical interactions between them, which culminates in a greater adsorption potential for hPAN@GO-SF membranes. Mansor et al. [75] stated that roughness, by affecting permeance and the tendency for membrane fouling, has a high impact on the adsorptive performance of membranes.

While in the batch tests for cationic dyes higher adsorption rates of the hPAN@GO-SF membranes were obtained for BB7 (200.4 $\text{mg}\cdot\text{g}^{-1}$) and MB (191.1 $\text{mg}\cdot\text{g}^{-1}$), in ultrafiltration assays higher performance was

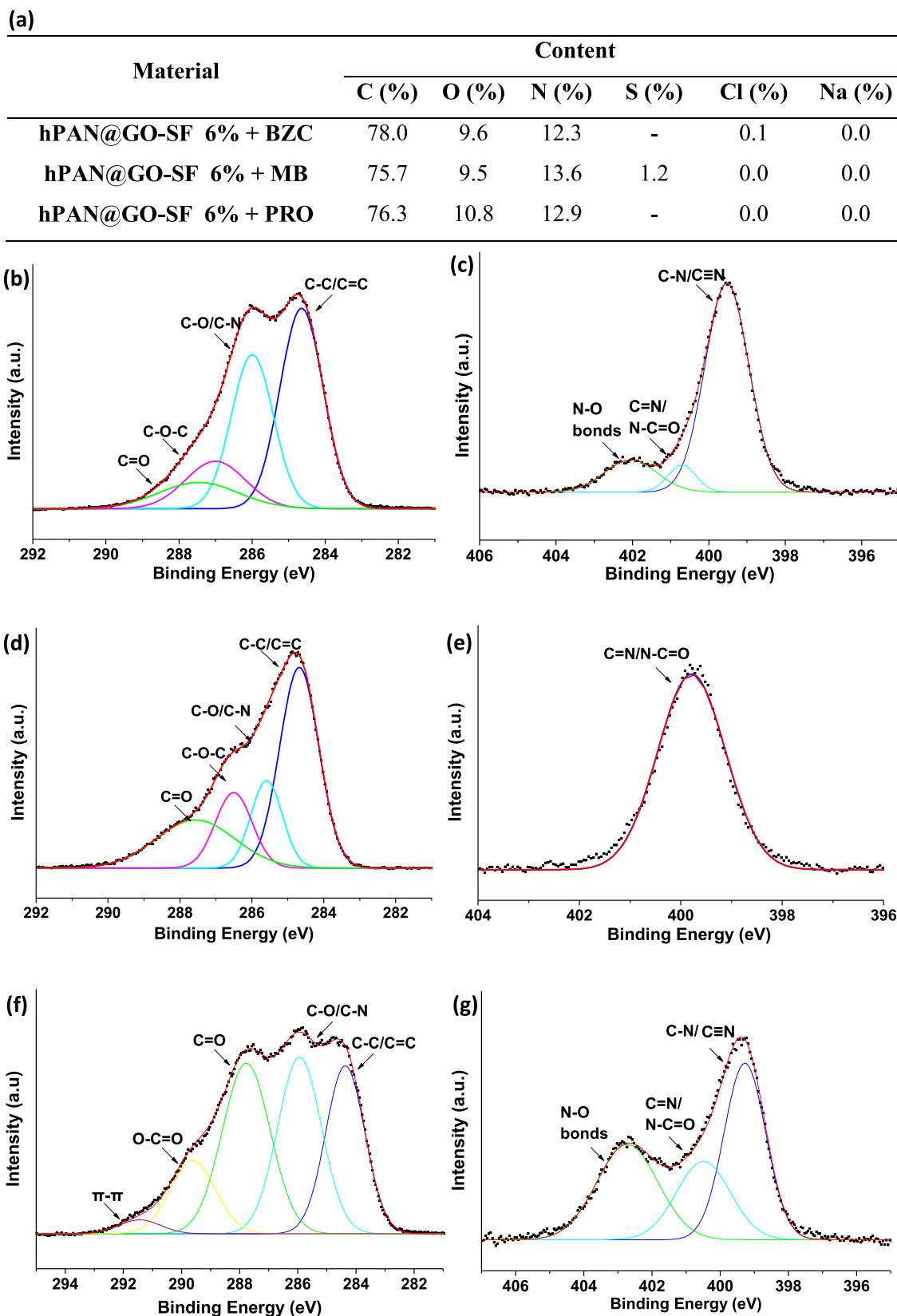


Fig. 9. (a) Data obtained for membranes by XPS survey; (b) C1s high-resolution XPS spectrum of hPAN@GO-SF 6% with BZC; (c) N1s high-resolution XPS spectrum of hPAN@GO-SF 6% with BZC; (d) C1s high-resolution XPS spectrum of hPAN@GO-SF 6% with MB (e) N1s high-resolution XPS spectrum of hPAN@GO-SF 6% with MB (f) C1s high-resolution XPS spectrum of hPAN@GO-SF 6% with PRO; (g) N1s high-resolution XPS spectrum of hPAN@GO-SF 6% with PRO;

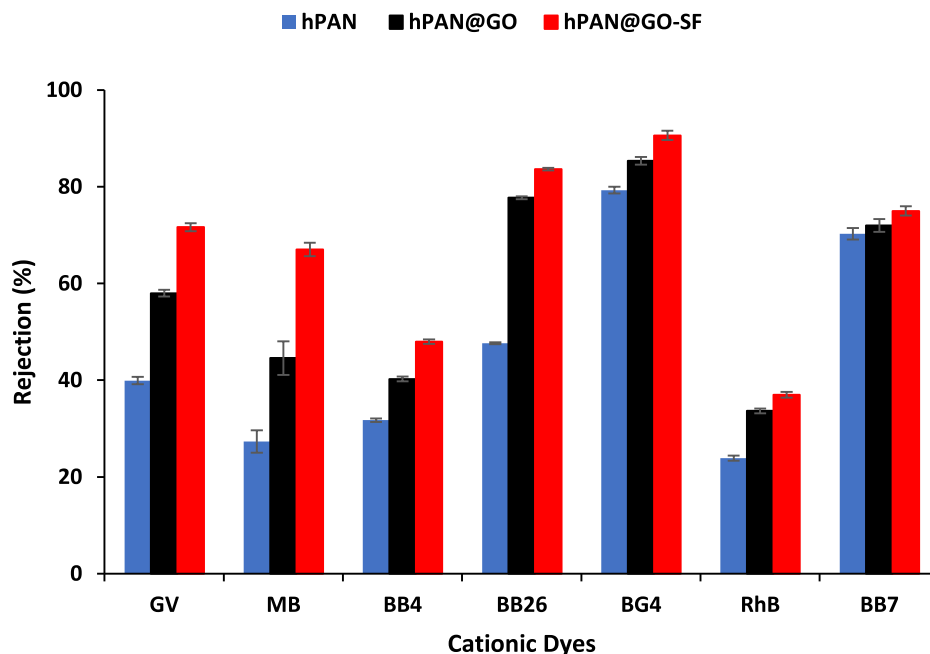


Fig. 10. Continuous flow adsorption of cationic dyes by hPAN (blue blocks), hPAN@GO (black blocks) and hPAN@GO-SF (red blocks) membranes. 6% of nano-material dosage of membranes, 5 cm average membrane diameter, cationic dyes initial concentration of 10 mg.L^{-1} , 50 mL of dye solution, 1 mL.min^{-1} of flux, pH 6 and at room temperature.

verified for the cationic dyes BB26 ($83.6\% \sim 225.6 \text{ mg.m}^{-2}$) and BG4 ($90.6\% \sim 246.7 \text{ mg.m}^{-2}$). These results suggest that the selectivity of membranes changes according to the adsorption process to which they are submitted. This indicates that in addition to parameters such as roughness index, porosity and hydrophilicity, adsorbent/adsorbate

interactions can be influenced by the adsorptive process. Hernández et al. [97] studied the adsorption rate of phenol on an activated carbon tissue, and found that hydrodynamics plays a relevant role in the adsorption process, mainly in laminar flows. This statement was also expressed by Wang et al. [98] who reported that at low agitation rates

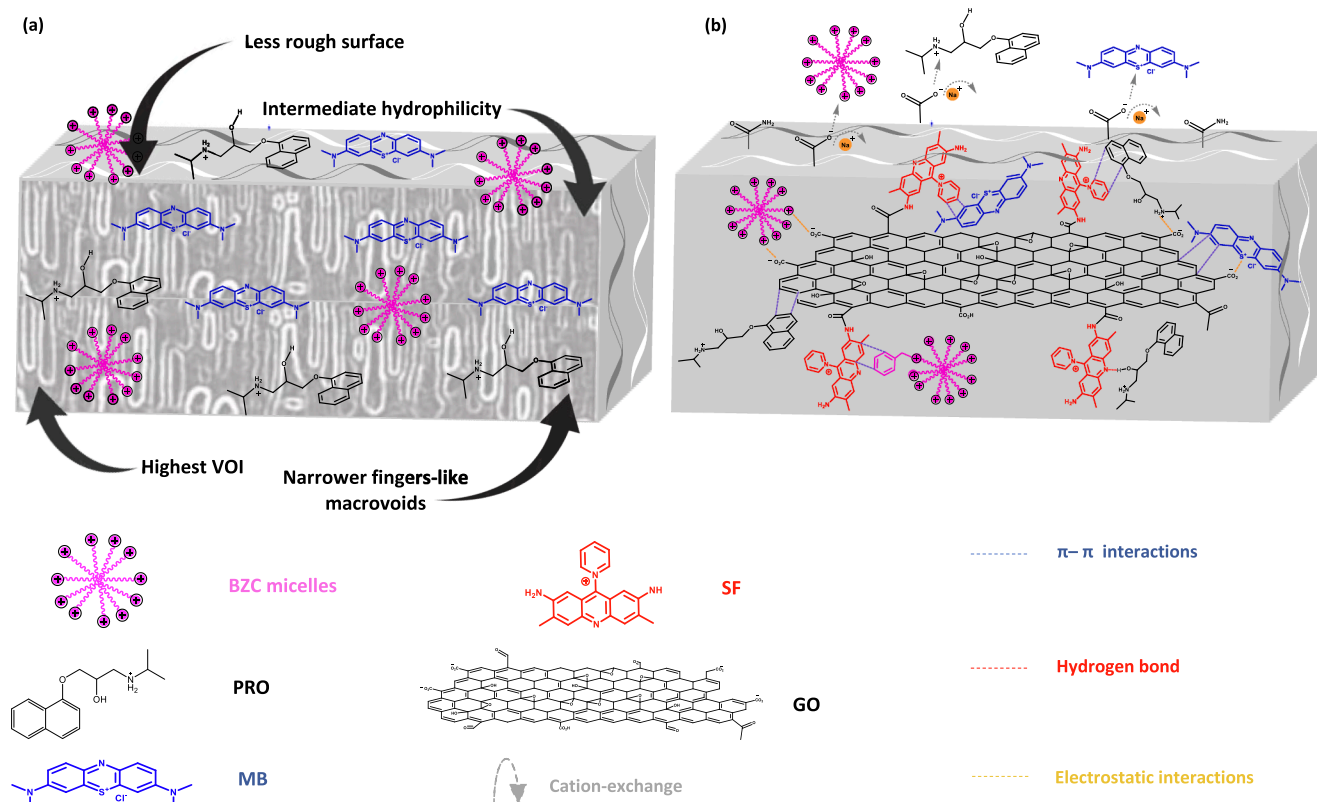


Fig. 11. (a) Morphological and (b) Physicochemical adsorption mechanisms of multiple organic contaminants into the hPAN@GO-SF.

there is greater heterogeneity of solutions, which limits solute distribution and makes the permeation flow uneven. Such phenomena can explain the differences in membrane selectivity in the two adsorptive processes, which have different solute flow profiles. While in direct flow the flow is laminar, in batch this process is characterized as turbulent.

3.4. Adsorption mechanisms of organic contaminants on hPAN based GO membranes

GO-SF incorporation in the polymeric matrix, by causing morphological and chemical changes in the pristine membrane, potentiated the ability to remove multiple organic contaminants in different flow profiles of hPAN. In terms of morphology, the nano-adsorbent reduced membrane surface roughness, modified the size and shape of the sublayers macrovoids, and increased the materials' hydrophilicity. These new conformations maintained a good PWF for hPAN@GO-SF and contributed to a better adhesion of contaminating molecules to the material. In the chemical bias, hPAN and GO-SF provided hydroxyl, carboxyl, epoxy and phenazinium groups to membranes, which contributed and potentiated electrostatic and π - π interactions and adsorbent/adsorbate hydrogen bonds [28] (Fig. 11).

In general, hPAN@GO-SF membranes exhibit maximum adsorption potential for contaminants of 200.6 mg.g⁻¹ for PRO, 191.1 mg.g⁻¹ for MB and 154.8 mg.g⁻¹ for BZC in batch assays, and in ultrafiltration reached 225.6 mg.m⁻² for BB6 and 246.7 mg.m⁻² for BG4 (Table 4). hPAN@GO-SF membranes achieved superior removal and filtration capacities when compared to other 3D materials described in the literature. In a practical application, the new membranes, in addition to good adsorption for multiple ECs, have good flexibility, which facilitates their handling and operation during adsorption processes [99].

4. Conclusions

The new proposed hydrolyzed polyacrylonitrile (hPAN) membranes containing GO and GO modified with the cationic dye safranin (GO-SF) were synthesized, fully characterized and applied to water treatment. hPAN@GO and hPAN@GO-SF were prepared using low-cost chemical reagents and classical chemical modifications and some structural elucidation was carried out to confirm the differences between both materials. The increase in interlayer spacing from GO to GO-SF in the XRD pattern, the presence of SF bands in the GO FTIR spectrum and the presence of N and Cl in the XPS analysis confirm the successful synthesis of GO-SF. Zeta potential demonstrated that GO-SF had a lower electronegative surface charge than GO due the presence of phenazinium

cations of SF in the nanomaterial matrix. Regarding the AFM in liquid media, SEM and MicroCT of new membranes, the analyses indicated that the addition of nanomaterial to the membrane modified the finger-like macrovoid sublayers, reduced surface roughness and increase VOI. The water contact angle analysis indicated that the hPAN@GO-SF membranes were more hydrophilic than others, reaching a maximum value of 6.95°. From the zeta potential analysis, it was found that even after the insertion of the phenazinium cation, hPAN@GO-SF still had an electronegative potential (-15.63 to -40.8 mV).

Batch experiments showed that hPAN@GO-SF had higher adsorption capacity compared to pristine hPAN and hPAN@GO membranes, with maximum adsorption potential for the drug PRO (200.6 mg.g⁻¹), the surfactant BZC (154.8 mg.g⁻¹), the cationic dye MB (200.4 mg.g⁻¹) and the anionic dye RBB (39.88 mg.g⁻¹) both at 100 mg.L⁻¹. DFT calculations, adsorption experiments in saline media and post adsorption XPS analysis showed that cation exchange, hydrogen bond, π - π and electrostatics interactions are common between adsorbent/adsorbate. The ultrafiltration experiments with hPAN@GO-SF presented better rejection rates than hPAN and hPAN@GO, achieving a maximum rejection to the cationic dyes BB26 (84% ~ 242.60 mg.m⁻²) and BG4 (90% ~ 237.39 mg.m⁻²). This difference is probably related to the lower mean square roughness of hPAN@GO-SF compared to hPAN and hPAN@GO membranes.

These results indicated that the adsorption potential of new membranes depends on three specific factors: chemical, morphological and permeance characteristics. Although these are unique parameters, their combination affects the selectivity of the membrane. Through chemical properties, GO-SF provides oxygenated, phenolic and phenazinium groups to the membranes which may have improved their adsorbent ability through π - π and electrostatic interactions, as well as, hydrogen-bonds between adsorbent/adsorbate. Regarding the morphological features of hPAN@GO-SF, it showed an asymmetrical and thickened finger-like macrovoid sublayer and a less rough surface, which contributed to better adhesion of the compounds to the material. And the change of membrane selectivity according to the adsorption process could be explained by the flow profile differences, as in laminar flow there is greater heterogeneity of solutions, which limits solute distribution and makes the permeation flow uneven. hPAN@GO-SF has a superior adsorption capacity for multiple ECs compared to other 3D materials and these results are encouraging, indicating that the modifications made to the membrane enhance its ability to remove contaminants from water. The present study guides to new insights on how the incorporation of adsorbents into polymeric materials affects the chemical and morphological properties of the membranes as well as their

Table 4

Comparison of hPAN@GO and hPAN@GO-SF adsorption capacity in batch experiments with other 3D adsorbents and ultrafiltration rejection rate.

Adsorbent	Contaminants	Morfology	pH	Temperature	q _m	Ref.
GVCP	BZC	Membrane	6	r.t.	0.94 mg.g ⁻¹	[100]
FTKNRL	BZC	Membrane	6	r.t.	2.00 mg.g ⁻¹	[100]
hPAN@GO	BZC	Membrane	6	r.t.	129.3 mg.g ⁻¹	This work
hPAN@GO-SF	BZC	Membrane	6	r.t.	154.8 mg.g ⁻¹	This work
PVDF/MWCNT	MB	Membrane	6	r.t.	4.4 mg.g ⁻¹	[101]
PLLA	MB	Membrane	6	20 °C	74.51 mg.g ⁻¹	[102]
hPAN@GO	MB	Membrane	6	r.t.	183.5 mg.g ⁻¹	This work
hPAN@GO-SF	MB	Membrane	6	r.t.	191.1 mg.g ⁻¹	This work
DMPA Liposome	PRO	Biomembrane	6	r.t.	155.6 mg.g ⁻¹	[103]
DMPC Liposome	PRO	Biomembrane	6	r.t.	181.5 mg.g ⁻¹	[103]
hPAN@GO	PRO	Membrane	6	r.t.	177.4 mg.g ⁻¹	This work
hPAN@GO-SF	PRO	Membrane	6	r.t.	200.6 mg.g ⁻¹	This work
Carbon/Ba/alginate	BB26	Beads	4	-	1.9 mg.g ⁻¹	[104]
Activated carbon (AC3-R2)	BB26	Beads	5.8	30 °C	76.0 mg.g ⁻¹	[105]
hPAN@GO	BB26	Membrane	6	r.t.	209.7 mg.m ⁻²	This work
hPAN@GO-SF	BB26	Membrane	6	r.t.	225.6 mg.m ⁻²	This work
Chitosan	BG4	Beads	8	35 °C	93.5 mg.g ⁻¹	[106]
CD/CMC	BG4	Granules	8	25 °C	91.9 mg.g ⁻¹	[107]
hPAN@GO	BG4	Membrane	6	r.t.	232.4 mg.m ⁻²	This work
hPAN@GO-SF	BG4	Membrane	6	r.t.	246.7 mg.m ⁻²	This work

performance in water purification.

CRedit authorship contribution statement

Tauany de Figueiredo Neves: Investigation, Methodology, Software, Validation, Formal analysis, Data curation, Writing – original draft. **Natália Gabriele Camparotto:** Software, Validation, Formal analysis, Data curation. **Everton Augusto Rodrigues:** Investigation, Methodology. **Valmor Roberto Mastelaro:** Formal analysis, Investigation. **Renato Falcão Dantas:** Supervision, Funding acquisition. **Patrícia Prediger:** Project administration, Formal analysis, Investigation, Resources, Data curation, Funding acquisition.

Declaration of Competing Interest

The authors declare that they have no known competing financial interests or personal relationships that could have appeared to influence the work reported in this paper.

Acknowledgements

This research was supported by The São Paulo Research Foundation (FAPESP, n. 2019/25228-0, 2019/07822-2 and 2013/07296-2), The National Council for Scientific and Technological Development (CNPq), Coordination for the Improvement of Higher Education Personnel (CAPES) (Finance Code 001) and Fund for Support to Teaching, Research and Outreach Activities (FAPEX, n. 2461/20). The authors are grateful to Brazilian Nanotechnology National Laboratory (LNNano, CNPEM) for the support provided in AFM in liquid media, MicroCT and Water contact angle analyses and Brazilian Biorenewables National Laboratory (LNBR, CNPEM) for the support provided in the Zeta potential analysis. We are grateful to Dra. Josiane Aparecida de Souza Vendemiatti and Dr. Ausdinir Danilo Borotolozo for the SEM and DRX analyses, respectively carried out at the Faculty of Technology and Faculty of Applied Sciences at UNICAMP-Limeira. The authors are thankful to Espaço da Escrita for the main article review & editing.

Appendix A. Supplementary data

Supplementary data to this article can be found online at <https://doi.org/10.1016/j.cej.2022.137176>.

References

- [1] K. Fijalkowski, Emerging contaminants in sludge (endocrine disruptors, pesticides, and pharmaceutical residues, including illicit drugs/controlled substances, etc.), *Ind. Munic. Sludge Emerg. Concerns Scope Resour. Recover.* (2019) 455–473, <https://doi.org/10.1016/B978-0-12-815907-1.00020-9>.
- [2] Sunaina, H. Kaur, N. Kumari, A. Sharma, M. Sachdeva, V. Mutreja, *Optical and electrochemical microfluidic sensors for water contaminants: A short review*, *Mater. Today Proc.* 48 (2022) 1673–1679.
- [3] A. Tkaczyk, K. Mitrowska, A. Posyniak, Synthetic organic dyes as contaminants of the aquatic environment and their implications for ecosystems: A review, *Sci. Total Environ.* 717 (2020), 137222, <https://doi.org/10.1016/j.scitotenv.2020.137222>.
- [4] M. Uygun, V. de la Asunción-Nadal, S. Evli, D.A. Uygun, B. Jurado-Sánchez, A. Escarpa, Dye removal by laccase-functionalized micromotors, *Appl. Mater. Today*. 23 (2021), 101045, <https://doi.org/10.1016/J.APMT.2021.101045>.
- [5] S. Mousavi, F. Shahraki, M. Aliabadi, A. Haji, F. Deuber, C. Adhart, Nanofiber immobilized CeO₂/dendrimer nanoparticles: An efficient photocatalyst in the visible and the UV, *Appl. Surf. Sci.* 479 (2019) 608–618, <https://doi.org/10.1016/J.APSUSC.2019.02.119>.
- [6] N.C. Dias, J.P. Bassin, G.L. Sant'Anna, M. Dezotti, Ozonation of the dye Reactive Red 239 and biodegradation of ozonation products in a moving-bed biofilm reactor: Revealing reaction products and degradation pathways, *Int. Biodeterior. Biodegradation*. 144 (2019), <https://doi.org/10.1016/J.IBIOD.2019.104742>, 104742.
- [7] T. de Figueiredo Neves, N. Barticiotto Dalarme, P.M.M. da Silva, R. Landers, C. Siqueira Franco Picone, P. Prediger, Novel magnetic chitosan/quaternary ammonium salt graphene oxide composite applied to dye removal, *J. Environ. Chem. Eng.* 8 (4) (2020), <https://doi.org/10.1016/j.jece.2020.103820>, 103820.
- [8] J. Yun, Y. Wang, Z. Liu, Y. Li, H. Yang, Z. liang Xu, High efficient dye removal with hydrolyzed ethanolamine-Polyacrylonitrile UF membrane: Rejection of anionic dye and selective adsorption of cationic dye, *Chemosphere*. 259 (2020) 127390, <https://doi.org/10.1016/J.CHEMOSPHERE.2020.127390>.
- [9] Y. Xu, G. Peng, J. Liao, J. Shen, C. Gao, Preparation of molecular selective GO/DTiO₂-PDA-PEI composite nanofiltration membrane for highly pure dye separation, 117727, *J. Memb. Sci.* 601 (2020), <https://doi.org/10.1016/J.MEMSCI.2019.117727>.
- [10] L. Xing, N. Guo, Y. Zhang, H. Zhang, J. Liu, A negatively charged loose nanofiltration membrane by blending with poly (sodium 4-styrene sulfonate) grafted SiO₂ via SI-ATRP for dye purification, *Sep. Purif. Technol.* 146 (2015) 50–59, <https://doi.org/10.1016/J.SEPPUR.2015.03.030>.
- [11] C. Yang, W. Xu, Y. Nan, Y. Wang, Y. Hu, C. Gao, X. Chen, Fabrication and characterization of a high performance polyimide ultrafiltration membrane for dye removal, *J. Colloid Interface Sci.* 562 (2020) 589–597, <https://doi.org/10.1016/J.JCIS.2019.11.075>.
- [12] R.S. Bhavsar, T. Mitra, D.J. Adams, A.I. Cooper, P.M. Budd, Ultrahigh-permeance PIM-1 based thin film nanocomposite membranes on PAN supports for CO₂ separation, *J. Memb. Sci.* 564 (2018) 878–886, <https://doi.org/10.1016/J.MEMSCI.2018.07.089>.
- [13] Y. Yang, S. Zhang, X. Zhao, J. Yu, B. Ding, Sandwich structured polyamide-6/polyacrylonitrile nanonets/bead-on-string composite membrane for effective air filtration, *Sep. Purif. Technol.* 152 (2015) 14–22, <https://doi.org/10.1016/J.SEPPUR.2015.08.005>.
- [14] Z. Liu, S. Ma, X. Li, H. Yang, Z. Xu, Porous carbonaceous composite derived from Mg(OH)₂ pre-filled PAN based membrane for supercapacitor and dye adsorption application, *J. Solid State Chem.* 277 (2019) 493–501, <https://doi.org/10.1016/J.JSSC.2019.07.007>.
- [15] Y. Mansourpanah, M. Samimi, Preparation and characterization of a low-pressure efficient polyamide multi-layer membrane for water treatment and dye removal, *J. Ind. Eng. Chem.* 53 (2017) 93–104, <https://doi.org/10.1016/J.JIEC.2017.04.007>.
- [16] Y. Li, Y. Wang, Z. Liu, L. Jiang, H. Yang, Z. Xu, Separation of anionic dye mixtures by Al-metal-organic framework filled polyacrylonitrile-ethanolamine membrane and its modified product, *J. Clean. Prod.* 284 (2021), 124778, <https://doi.org/10.1016/J.JCLEPRO.2020.124778>.
- [17] P. Bahmani, A. Maleki, H. Daraei, M. Khamforoush, R. Rezaee, F. Gharibi, A. G. Tkachev, A.E. Burakov, S. Agarwal, V.K. Gupta, High-flux ultrafiltration membrane based on electrospun polyacrylonitrile nanofibrous scaffolds for arsenate removal from aqueous solutions, *J. Colloid Interface Sci.* 506 (2017) 564–571, <https://doi.org/10.1016/J.JCIS.2017.07.086>.
- [18] M. Hu, B. Mi, Layer-by-layer assembly of graphene oxide membranes via electrostatic interaction, *J. Memb. Sci.* 469 (2014) 80–87, <https://doi.org/10.1016/j.memsci.2014.06.036>.
- [19] Y.X. Wang, Y.J. Li, H. Yang, Z.L. Xu, Super-wetting, photoactive TiO₂ coating on amino-silane modified PAN nanofiber membranes for high efficient oil-water emulsion separation application, *J. Memb. Sci.* 580 (2019) 40–48, <https://doi.org/10.1016/J.MEMSCI.2019.02.062>.
- [20] B. Zhang, D. Wang, Y. Wu, Z. Wang, T. Wang, J. Qiu, Modification of the desalination property of PAN-based nanofiltration membranes by a preoxidation method, *Desalination*. 357 (2015) 208–214, <https://doi.org/10.1016/J.DESAL.2014.12.004>.
- [21] Y. Ren, Y. Gu, Q. Zeng, Y. Zhang, UV-induced surface grafting polymerization for preparing phosphorus-containing flame retardant polyacrylonitrile fabric, *Eur. Polym. J.* 94 (2017) 1–10, <https://doi.org/10.1016/J.EURPOLYMJ.2017.06.037>.
- [22] Z. Yu, Y. Zhao, B. Gao, X. Liu, L. Jia, F. Zhao, J. Ma, Performance of novel Ag-nTiO₂/PVC reinforced hollow fiber membrane applied in water purification: in situ antibacterial properties and resistance to biofouling, *RSC Adv.* 5 (2015) 97320–97329, <https://doi.org/10.1039/C5RA18185B>.
- [23] H. Ju, B.D. McCloskey, A.C. Sagle, Y.H. Wu, V.A. Kusuma, B.D. Freeman, Crosslinked poly(ethylene oxide) fouling resistant coating materials for oil/water separation, *J. Memb. Sci.* 307 (2008) 260–267, <https://doi.org/10.1016/J.MEMSCI.2007.09.028>.
- [24] D.I. Petukhov, O.O. Kapitanova, E.A. Eremina, E.A. Goodilin, Preparation, chemical features, structure and applications of membrane materials based on graphene oxide, *Mendeleev Commun.* 31 (2021) 137–148, <https://doi.org/10.1016/J.MENCOM.2021.03.001>.
- [25] N.C. Homem, N. de Camargo Lima, S. Beluci, R. Amorim, A.M.S. Reis, M.F. Vieira, R. Vieira, M.T.P.A. Bergamasco, Surface modification of a polyethersulfone microfiltration membrane with graphene oxide for reactive dyes removal, *Appl. Surf. Sci.* 486 (2019) 499–507, <https://doi.org/10.1016/J.APSUSC.2019.04.276>.
- [26] M. Yang, C. Zhao, S. Zhang, P. Li, D. Hou, Preparation of graphene oxide modified poly(m-phenylene isophthalamide) nanofiltration membrane with improved water flux and antifouling property, *Appl. Surf. Sci.* 394 (2017) 149–159, <https://doi.org/10.1016/J.APSUSC.2016.10.069>.
- [27] E.F. Diogo Januário, N. de Camargo Lima, T.B. Beluci, M.F. Vidovix, R. Vieira, A. M. Salcedo Vieira, Functionalization of membrane surface by layer-by-layer assembly method for dyes removal, *Process Saf. Environ. Prot.* 134 (2020) 140–148, <https://doi.org/10.1016/J.PSEP.2019.11.030>.
- [28] E.F.D. Januário, T.B. Vidovix, N.d.C.L. Beluci, R.M. Paixão, L.H.B.R.d. Silva, N. C. Homem, R. Bergamasco, A.M.S. Vieira, Advanced graphene oxide-based membranes as a potential alternative for dyes removal: A review, *Sci. Total Environ.* 789 (2021), <https://doi.org/10.1016/J.SCITOTENV.2021.147957>, 147957.
- [29] J. Chen, H. Wu, G. Sheng, H. Li, M. Li, X. Guo, H. Dong, Graphene oxide-mediated the reduction of U(VI), Re(VII), Se(VI) and Se(IV) by Fe(II) in aqueous solutions

- investigated via combined batch, DFT calculation and spectroscopic approaches, *Chem. Eng. J.* 433 (2022), <https://doi.org/10.1016/J.CEJ.2021.133844>, 133844.
- [30] K. Juegchareonpoon, P. Wanichpongpan, V. Boonamnuayvitaya, Trimethoprim adsorption using graphene oxide-carboxymethylcellulose film coated on polyethylene terephthalate as a supporter, 108641, *Chem. Eng. Process. - Process Intensif.* 169 (2021), <https://doi.org/10.1016/J.CEP.2021.108641>.
- [31] L. Liu, B. Zhang, Y. Zhang, Y. He, L. Huang, S. Tan, X. Cai, Simultaneous Removal of Cationic and Anionic Dyes from Environmental Water Using Montmorillonite-Pillared Graphene Oxide, *J. Chem. Eng. Data.* 60 (2015) 1270–1278, <https://doi.org/10.1021/JE5009312>.
- [32] X. Zhang, C. Qin, Y. Gong, Y. Song, G. Zhang, R. Chen, Y. Gao, L. Xiao, S. Jia, Co-adsorption of an anionic dye in the presence of a cationic dye and a heavy metal ion by graphene oxide and photo-reduced graphene oxide, *RSC Adv.* 9 (2019) 5313–5324, <https://doi.org/10.1039/C8RA09438A>.
- [33] I. Chandio, F.A. Janjhi, A.A. Memon, S. Memon, Z. Ali, K.H. Thebo, A.A. A. Pirzado, A.A. Hakro, W.S. Khan, Ultrafast ionic and molecular sieving through graphene oxide based composite membranes, 114848, *Desalination.* 500 (2021), <https://doi.org/10.1016/J.DESAL.2020.114848>.
- [34] F. Ahmed Janjhi, I. Chandio, A. Ali Memon, Z. Ahmed, K. Hussain Thebo, A. Ali Ayaz Pirzado, A. Ali Hakro, M. Iqbal, Functionalized graphene oxide based membranes for ultrafast molecular separation, *Sep. Purif. Technol.* 274 (2021), <https://doi.org/10.1016/J.SEPPUR.2020.117969>.
- [35] Q. Zhang, X. Qian, K.H. Thebo, H.M. Cheng, W. Ren, Controlling reduction degree of graphene oxide membranes for improved water permeance, *Sci. Bull.* 63 (2018) 788–794, <https://doi.org/10.1016/J.SCI.2018.05.015>.
- [36] L. Chen, Y. Li, L. Chen, N. Li, C. Dong, Q. Chen, B. Liu, Q. Ai, P. Si, J. Feng, L. Zhang, J. Suhr, J. Lou, L. Ci, A large-area free-standing graphene oxide multilayer membrane with high stability for nanofiltration applications, *Chem. Eng. J.* 345 (2018) 536–544, <https://doi.org/10.1016/j.cej.2018.03.136>.
- [37] T.N. Magalhães de Paula, J.A. Souza Vendemiatti, N.G. Camparotto, B. Toledo, Á. C. Oliveira, T.F. Neves, G.A. Muzubeiro, P. Prediger, Behavior of two classes of organic contaminants in the presence of graphene oxide: Ecotoxicity, physicochemical characterization and theoretical calculations, 153515, *Sci. Total Environ.* 822 (2022), <https://doi.org/10.1016/J.SCI.2022.153515>.
- [38] T. de Figueiredo Neves, P. Kushima Assano, L. Rodrigues Sabino, W. Bardelin Nunes, P. Prediger, Influence of Adsorbent/Adsorbate Interactions on the Removal of Cationic Surfactants from Water by Graphene Oxide, *Water, Air, Soil Pollut.* 231 (2020) 1–22, <https://doi.org/10.1007/s11270-020-04669-w>.
- [39] P. Prediger, T. Cheminski, T. de Figueiredo Neves, W.B. Nunes, L. Sabino, C.S. F. Picone, R.L. Oliveira, C.R.D. Correia, Graphene oxide nanomaterials for the removal of non-ionic surfactant from water, *J. Environ. Chem. Eng.* 6 (2018) 1536–1545, <https://doi.org/10.1016/j.jece.2018.01.072>.
- [40] M.K. Sahu, U.K. Sahu, R.K. Patel, Correction: Adsorption of safranin-O dye on CO₂ neutralized activated red mud waste: Process modelling, analysis and optimization using statistical design, *RSC Adv.* 5 (2015) 4229–42302, <https://doi.org/10.1039/c5ra00033j>.
- [41] E. Albitser, S. Alfaro, M.A. Valenzuela, Photosensitized oxidation of 9,10-dimethylanthracene with singlet oxygen by using a safranin O/silica composite under visible light, *Photochem. Photobiol. Sci.* 14 (2015) 597–602, <https://doi.org/10.1039/c4pp00261j>.
- [42] C.S. Bhatt, B. Nagaraj, A.K. Suresh, Nanoparticles-shape influenced high-efficient degradation of dyes: Comparative evaluation of nano-cubes vs nano-rods vs nano-spheres, *J. Mol. Liq.* 242 (2017) 958–965, <https://doi.org/10.1016/J.MOLLIQ.2017.07.101>.
- [43] P.R. Young, *Practical Spectroscopy: the Rapid Interpretation of Spectral Data*, 2000. https://www.google.com.br/books/edition/Practical_Spectroscopy_the_Rapid_Interpr/Sh0uQEACAAJ?hl=pt-BR (accessed April 27, 2022).
- [44] P. Bernardo, G. Clarizia, Enhancing Gas Permeation Properties of Pebax® 1657 Membranes via Polysorbate Nonionic Surfactants Doping, *Polymers (Basel)*. 12 (2020) 253, <https://doi.org/10.3390/polym12020253>.
- [45] M. Varga, T. Izak, V. Vretenar, H. Kozak, J. Holovsky, A. Artemenko, M. Hulman, V. Skakalova, D.S. Lee, A. Kromka, Diamond/carbon nanotube composites: Raman, FTIR and XPS spectroscopic studies, *Carbon N. Y.* 111 (2017) 54–61, <https://doi.org/10.1016/j.carbon.2016.09.064>.
- [46] V.R. Moreira, Y.A.R. Lebron, M.M. da Silva, L.V. de Souza Santos, R.S. Jacob, C.K. B. de Vasconcelos, M.M. Viana, Graphene oxide in the remediation of norfloxacin from aqueous matrix: simultaneous adsorption and degradation process, *Environ. Sci. Pollut. Res.* 27 (2020) 34513–34528, <https://doi.org/10.1007/S11356-020-09656-6/TABLES/7>.
- [47] A. Schöll, Y. Zou, M. Jung, T. Schmidt, R. Fink, E. Umbach, Line shapes and satellites in high-resolution x-ray photoelectron spectra of large pi-conjugated organic molecules, *J. Chem. Phys.* 121 (2004) 10260–10267, <https://doi.org/10.1063/1.1807812>.
- [48] H. Lv, H. Zhang, G. Ji, H. Lv, H. Zhang, G. Ji, Development of Novel Graphene/g-C₃N₄ Composite with Broad-Frequency and Light-Weight Features, *Part. Part. Syst. Charact.* 33 (2016) 656–663, <https://doi.org/10.1002/PPSC.201600065>.
- [49] A. Manakhov, L. Zajíčková, M. Eliáš, J. Čechal, J. Polčák, J. Hnilica, S. Bittnerová, D. Nečas, Optimization of Cyclopropylamine Plasma Polymerization toward Enhanced Layer Stability in Contact with Water, *Plasma Process. Polym.* 11 (2014) 532–544, <https://doi.org/10.1002/PPAP.201300177>.
- [50] S. Gurunathan, J.W. Han, E. Kim, D. Kwon, J. Park, J. Kim, Enhanced green fluorescent protein-mediated synthesis of biocompatible graphene, *J. Nanobiotechnology.* 12 (2014), <https://doi.org/10.1186/s12951-014-0041-9>.
- [51] H. Zhang, L. Quan, A. Gao, Y. Tong, F. Shi, L. Xu, The Structure and Properties of Polyacrylonitrile Nascent Composite Fibers with Grafted Multi Walled Carbon Nanotubes Prepared by Wet Spinning Method, *Polymers* 11 (2019) 422, <https://doi.org/10.3390/POLYM11030422>.
- [52] D.A. Skoog, F.J. Holler, S.R. Crouch, Principles of instrumental analysis, 1992. <https://search.library.wisc.edu/catalog/999674775302121/cite> (accessed September 3, 2021).
- [53] M. Dutta, S. Bhattacharjee, S. De, Separation of reactive dyes from textile effluent by hydrolyzed polyacrylonitrile hollow fiber ultrafiltration quantifying the transport of multicomponent species through charged membrane pores, *Sep. Purif. Technol.* 234 (2020), 116063, <https://doi.org/10.1016/j.seppur.2019.116063>.
- [54] L. Pérez-Álvarez, L. Ruiz-Rubio, I. Moreno, J.L. Vilas-Vilela, Characterization and optimization of the alkaline hydrolysis of polyacrylonitrile membranes, *Polymers (Basel)*. 11 (2019) 1–11, <https://doi.org/10.3390/polym11111843>.
- [55] K. Müller, M. Richter, D. Friedrich, I. Paloumpa, U.I. Kramm, D. Schmeißer, Spectroscopic characterization of Cobalt-Phthalocyanine electrocatalysts for fuel cell applications, *Solid State Ionics.* 216 (2012) 78–82, <https://doi.org/10.1016/J.SSI.2011.12.013>.
- [56] S. Ravi, S. Zhang, Y.R. Lee, K.K. Kang, J.M. Kim, J.W. Ahn, W.S. Ahn, EDTA-functionalized KCC-1 and KIT-6 mesoporous silicas for Nd³⁺ ion recovery from aqueous solutions, *J. Ind. Eng. Chem.* 67 (2018) 210–218, <https://doi.org/10.1016/J.JIEC.2018.06.031>.
- [57] S. Deng, R. Bai, Removal of trivalent and hexavalent chromium with aminated polyacrylonitrile fibers: performance and mechanisms, *Water Res.* 38 (2004) 2424–2432, <https://doi.org/10.1016/J.WATRES.2004.02.024>.
- [58] T. Tavangar, A. Hemmati, M. Karimi, F. Zokaei Ashtiani, Layer-by-layer assembly of graphene oxide (GO) on sulfonated polyethersulfone (SPES) substrate for effective dye removal, *Polym. Bull.* 76 (2019) 35–52, <https://doi.org/10.1007/S00289-018-2357-3/FIGURES/10>.
- [59] R.A. Dias, V. Da Nóbrega Medeiros, B.I.A. Silva, E.M. Araújo, H. De Lucena Lira, Study of the influence of viscosity on the morphology of polyethersulfone hollow fiber membranes/additives, *Mater. Res.* 22 (2020) 1–9, <https://doi.org/10.1590/1980-5373-MR-2018-0913>.
- [60] Z. Qiu, X. Ji, C. He, Fabrication of a loose nanofiltration candidate from Polyacrylonitrile/Graphene oxide hybrid membrane via thermally induced phase separation, *J. Hazard. Mater.* 360 (2018) 122–131, <https://doi.org/10.1016/J.JHAZMAT.2018.08.004>.
- [61] Z. Zhu, L. Wang, Y. Xu, Q. Li, J. Jiang, X. Wang, Preparation and characteristics of graphene oxide-blending PVDF nanohybrid membranes and their applications for hazardous dye adsorption and rejection, *J. Colloid Interface Sci.* 504 (2017) 429–439, <https://doi.org/10.1016/j.jcis.2017.05.068>.
- [62] T.A. Otitaju, M. Ahmadipour, S. Li, N.F. Shoparwe, L.X. Jie, A.L. Owlabi, Influence of nanoparticle type on the performance of nanocomposite membranes for wastewater treatment, *J. Water Process Eng.* 36 (2020), 101356, <https://doi.org/10.1016/J.JWPE.2020.101356>.
- [63] M.F. Twibi, M.H.D. Othman, S.K. Hubadillah, S.A. Alftessi, M.R.B. Adam, A. F. Ismail, A.M. Rahman, J. Jaafar, Y.O. Raji, M.H. Abd Aziz, M.N.B.M. Sokri, H. Abdullah, R. Naim, Hydrophobic mullite ceramic hollow fibre membrane (Hy-MFMD) for seawater desalination via direct contact membrane distillation (DCMD), *J. Eur. Ceram. Soc.* 41 (13) (2021) 6578–6585.
- [64] Y. Mansourpanah, A. Ghanbari, H. Yazdani, A.G. Mohammadi, A. Rahimpour, Silver-polyamidoamine/graphene oxide thin film nanofiltration membrane with improved antifouling and antibacterial properties for water purification and desalination, *Desalination.* 511 (2021), 115109, <https://doi.org/10.1016/J.DESAL.2021.115109>.
- [65] R. Asmatulu, Highly Hydrophilic Electrospun Polyacrylonitrile/Polyvinylpyrrolidone Nanofibers Incorporated with Gentamicin as Filter Medium for Dam Water and Wastewater Treatment, *J. Membr. Sep. Technol.* 5 (2016) 38–56, <https://doi.org/10.6000/1929-6037.2016.05.02.1>.
- [66] M. Nawaz, M.U. Islam, M.A. Nazir, I. Bano, I.H. Gul, M. Ajmal, Transport properties in spinel ferrite/graphene oxide nanocomposites for electromagnetic shielding, *Ceram. Int.* 47 (18) (2021) 25505–25513.
- [67] T. Cheminski, T. de Figueiredo Neves, P.M. Silva, C.H. Guimarães, P. Prediger, Insertion of phenyl ethylene glycol units on graphene oxide as stabilizers and its application for surfactant removal, *J. Environ. Chem. Eng.* 7 (2) (2019) 102976.
- [68] N.d.C.L. Beluci, N.C. Homem, M.T.S.P. Amorim, R. Bergamasco, A.M.S. Vieira, Biopolymer extracted from Moringa oleifera Lam. in conjunction with graphene oxide to modify membrane surfaces, *Environmental Technology* 41 (23) (2020) 3069–3080.
- [69] E. Valamohammadi, F. Behdarvand, M.A. Tofighy, T. Mohammadi, Preparation of positively charged thin-film nanocomposite membranes based on the reaction between hydrolyzed polyacrylonitrile containing carbon nanomaterials and HPEI for water treatment application, 116826, *Sep. Purif. Technol.* 242 (2020), <https://doi.org/10.1016/J.SEPPUR.2020.116826>.
- [70] R. Hou, Y. He, H. Yu, J. Ma, Y. Gao, Y. Bai, J. Chen, Intercalation of N-doped graphene into graphene oxide-based membranes to improve their overall nanofiltration performance, 138657, *Chem. Phys. Lett.* 775 (2021), <https://doi.org/10.1016/J.CPLETT.2021.138657>.
- [71] J. Men, H. Shi, C. Dong, Y. Yang, Y. Han, R. Wang, Y. Zhang, T. Zhao, J. Li, Preparation of poly(sodium 4-styrene sulfonate) grafted magnetic chitosan microspheres for adsorption of cationic dyes, *Int. J. Biol. Macromol.* 181 (2021) 810–823, <https://doi.org/10.1016/J.IJBIOMAC.2021.04.079>.
- [72] M.R. Teixeira, M.J. Rosa, M. Nyström, The role of membrane charge on nanofiltration performance, *J. Membr. Sci.* 265 (2005) 160–166, <https://doi.org/10.1016/J.MEMSCI.2005.04.046>.

- [73] S. Wang, Z. Wen, S. Shi, W. Hou, Preparation and oil absorption performance of polyacrylonitrile / reduced graphene oxide composite porous material, *102092*, *J. Water Process Eng.* 41 (2021), <https://doi.org/10.1016/j.jwpe.2021.102092>.
- [74] W. Wu, Y. Shi, G. Liu, X. Fan, Y. Yu, Recent development of graphene oxide based forward osmosis membrane for water treatment: A critical review, *114452*, *Desalination*. 491 (2020), <https://doi.org/10.1016/j.desal.2020.114452>.
- [75] E.S. Mansor, H. Ali, A. Abdel-Karim, Efficient and reusable polyethylene oxide/polyaniline composite membrane for dye adsorption and filtration, *100314*, *Colloid Interface Sci. Commun.* 39 (2020), <https://doi.org/10.1016/j.COLCOM.2020.100314>.
- [76] A.G. Zestos, H. Chen, Effect of Surface Roughness on Electrochemical Adsorption/Desorption of Dopamine by Carbonaceous Electrodes, *ChemRxiv*. Cambridge Open Engag. 9 (2021) 66–68, <https://doi.org/10.11216/kokusajosei1988.9.66>.
- [77] M.S. Lord, J.M. Whitelock, A. Simmons, R.L. Williams, B.K. Milthorpe, Fibrinogen adsorption and platelet adhesion to silica surfaces with stochastic nanoporography, *Biointerphases*. 9 (4) (2014), <https://doi.org/10.1116/1.4900993>, 041002.
- [78] A. Deepatana, M. Valix, Steric hindrance effect on adsorption of metal-organic complexes onto aminophosphonate chelating resin, *Desalination*. 218 (2008) 297–303, <https://doi.org/10.1016/j.DESAL.2007.02.025>.
- [79] W.T. Vieira, M.D. Bispo, S. de Melo Farias, A.d.S.V. de Almeida, T.L. da Silva, M. G.A. Vieira, J.I. Soletti, T.L. Balliano, Activated carbon from macauba endocarp (*Acrocomia aculeate*) for removal of atrazine: Experimental and theoretical investigation using descriptors based on DFT, *J. Environ. Chem. Eng.* 9 (2) (2021), <https://doi.org/10.1016/j.JECE.2021.105155>, 105155.
- [80] M.M. Talmaciu, E. Bodoki, R. Oprean, Global chemical reactivity parameters for several chiral beta-blockers from the Density Functional Theory viewpoint, *Clujul Med.* 89 (2016) 513–518, <https://doi.org/10.15386/CJMED-610>.
- [81] R.G. Parr, R.G. Pearson, Absolute hardness: companion parameter to absolute electronegativity, *J. Am. Chem. Soc.* 105 (2002) 7512–7516, <https://doi.org/10.1021/JA00364A005>.
- [82] R.G. Pearson, Chemical hardness and the electronic chemical potential, *Inorganica Chim. Acta*. 198–200 (1992) 781–786, [https://doi.org/10.1016/S0020-1693\(00\)92423-X](https://doi.org/10.1016/S0020-1693(00)92423-X).
- [83] P.K. Chattaraj, U. Sarkar, D.R. Roy, Electrophilicity Index, *Chem. Rev.* 106 (2006) 2065–2091, <https://doi.org/10.1021/CR040109F>.
- [84] P. Mazumdar, D. Choudhury, Study of the alkyl- π interaction between methane and few substituted pyrimidine systems using DFT, AIM and NBO calculations, *113560*, *Comput. Theor. Chem.* 1208 (2022), <https://doi.org/10.1016/j.comptc.2021.113560>.
- [85] M.P. Boneva, K.D. Danov, N.C. Christov, P.A. Kralchevsky, Attraction between particles at a liquid interface due to the interplay of gravity- And electric-field-induced interfacial deformations, *Langmuir*. 25 (2009) 9129–9139, https://doi.org/10.1021/LA9006873/SUPPL_FILE/LA9006873_SI_003.AVI.
- [86] O. Gereben, L. Pusztai, Hydrogen bond connectivities in water-ethanol mixtures: On the influence of the H-bond definition, *J. Mol. Liq.* 220 (2016) 836–841, <https://doi.org/10.1016/J.MOLLIQ.2016.05.035>.
- [87] P.M. Silva, N.G. Camparotto, T.F. Neves, K.T.G. Lira, V.R. Mastelaro, C.S. F. Picone, P. Prediger, Effective removal of basic dye onto sustainable chitosan beads : Batch and fixed-bed column adsorption, beads stability and mechanism, *100348*, *Sustain. Chem. Pharm.* 18 (2020), <https://doi.org/10.1016/j.scp.2020.100348>.
- [88] M. Iqbal, A. Saeed, S.I. Zafar, FTIR spectrophotometry, kinetics and adsorption isotherms modeling, ion exchange, and EDX analysis for understanding the mechanism of Cd²⁺ and Pb²⁺ removal by mango peel waste, *J. Hazard. Mater.* 164 (2009) 161–171, <https://doi.org/10.1016/J.JHAZMAT.2008.07.141>.
- [89] J.E. House, K.A. House, *The Group IA and IIA Metals*, Academic Press (2016), <https://doi.org/10.1016/B978-0-12-804697-5.00008-7>.
- [90] P.M.M. da Silva, N.G. Camparotto, T. Figueiredo Neves, V.R. Mastelaro, B. Nunes, C. Siqueira Franco Picone, P. Prediger, Instantaneous adsorption and synergic effect in simultaneous removal of complex dyes through nanocellulose/graphene oxide nanocomposites: Batch, fixed-bed experiments and mechanism, *Environ. Nanotechnology, Monit. Manag.* 16 (2021) 100584.
- [91] Q. Yao, B. Fan, Y. Xiong, C. Jin, Q. Sun, C. Sheng, 3D assembly based on 2D structure of Cellulose Nanofibril/Graphene Oxide Hybrid Aerogel for Adsorptive Removal of Antibiotics in Water, *Sci. Rep.* 7 (2017) 1–13, <https://doi.org/10.1038/srep45914>.
- [92] G. Meilli, K.H. Adolffson, A. Impagnatiello, G. Rizza, M. Hakkarainen, G. Melilli, K.H. Adolffson, M. Hakkarainen, A. Impagnatiello, G. Rizza, Intriguing Carbon Flake Formation during Microwave-Assisted Hydrothermal Carbonization of Sodium Lignosulfonate, *Glob. Challenges*. 4 (2020) 1900111, <https://doi.org/10.1002/GCH2.201900111>.
- [93] S.E. Wheeler, Understanding substituent effects in noncovalent interactions involving aromatic rings, *Acc. Chem. Res.* 46 (2013) 1029–1038, https://doi.org/10.1021/AR300109N/ASSET/IMAGES/LARGE/AR-2012-00109N_0010.JPEG.
- [94] J. Zheng, L. Xia, S. Song, Electroosorption of Pb(II) in water using graphene oxide-bearing nickel foam as the electrodes, *RSC Adv.* 7 (2017) 23543–23549, <https://doi.org/10.1039/C7RA02956J>.
- [95] A. Majumdar, S.C. Das, T. Shripathi, R. Hippler, Chemical synthesis and surface morphology of amorphous hydrogenated carbon nitride film deposited by N₂/CH₄ dielectric barrier discharge plasma, *Composite Interfaces* 19 (3–4) (2012) 161–170.
- [96] S.M. Alardhi, T.M. Albayati, J.M. Alrubaye, A hybrid adsorption membrane process for removal of dye from synthetic and actual wastewater, *Chem. Eng. Process. - Process Intensif.* 157 (2020), <https://doi.org/10.1016/J.CEP.2020.108113>, 108113.
- [97] E. García-Hernández, C.G. Aguilar-Madera, E.C. Herrera-Hernández, R. Ocampo-Pérez, E. Bailón-García, F.B. Cortés, Hydrodynamic effects on the overall adsorption rate of phenol on activated carbon cloth through the advection-diffusion model application, *J. Ind. Eng. Chem.* 93 (2021) 267–278, <https://doi.org/10.1016/J.JIEC.2020.10.003>.
- [98] P. Wang, T. Reviol, S. Kluck, P. Würtz, M. Böhle, Mixing of non-Newtonian fluids in a cylindrical stirred vessel equipped with a novel side-entry propeller, *Chem. Eng. Sci.* 190 (2018) 384–395, <https://doi.org/10.1016/J.CES.2018.06.034>.
- [99] X. Wang, J. Dong, C. Gong, S. Zhang, J. Yang, A. Zhang, Z. Feng, Bendable poly(vinylidene fluoride)/polydopamine/ β -cyclodextrin composite electrospun membranes for highly efficient and bidirectional adsorption of cation and anion dyes from aqueous media, *109256*, *Compos. Sci. Technol.* 219 (2022), <https://doi.org/10.1016/J.COMPSCITECH.2021.109256>.
- [100] T. Bin, A.K. Kulshreshtha, R. Al-Shakhshir, S.L. Hem, Adsorption of benzalkonium chloride by filter membranes: Mechanisms and effect of formulation and processing parameters, *Pharm. Dev. Technol.* 4 (1999) 151–165, <https://doi.org/10.1081/PDT-100101350>.
- [101] Y. Huan, Z. Li, C. Li, G. Li, Adsorption performances of Methylene blue by poly(vinylidene fluoride)/MWCNT membranes via ultrasound-assisted phase inversion method, *Desalination*. *Water Treat.* 163 (2019) 83–95, <https://doi.org/10.5004/dwt.2019.24565>.
- [102] N. Mohammad, Y. Atassi, Adsorption of methylene blue onto electrospun nanofibrous membranes of polylactic acid and polyacrylonitrile coated with chloride doped polyaniline, *Sci. Reports* 2020 101 (10) (2020) 1–19, <https://doi.org/10.1038/s41598-020-69825-y>.
- [103] T. Ishigami, M.S. Chern, K. Suga, Y. Okamoto, H. Umakoshi, Adsorption behavior of propranolol on negatively-charged liposomes and its influence on membrane fluidity and polarity, *J. Nanosci. Nanotechnol.* 17 (2017) 1721–1728, <https://doi.org/10.1166/jnn.2017.12823>.
- [104] M. Kumar, R. Tamilarasan, V. Sivakumar, Adsorption of Victoria blue by carbon/Ba/alginate beads: Kinetics, thermodynamics and isotherm studies, *Carbohydr. Polym.* 98 (2013) 505–513, <https://doi.org/10.1016/J.CARBPOL.2013.05.078>.
- [105] T.N.V. de Souza, S.M.L. de Carvalho, M.G.A. Vieira, M.G.C. da Silva, D. do S. B. Brasil, Adsorption of basic dyes onto activated carbon: Experimental and theoretical investigation of chemical reactivity of basic dyes using DFT-based descriptors, *Appl. Surf. Sci.* 448 (2018) 662–670, <https://doi.org/10.1016/J.APSUSC.2018.04.087>.
- [106] Z. Bekçi, C. Özveri, Y. Seki, K. Yurdakoç, Sorption of malachite green on chitosan bead, *J. Hazard. Mater.* 154 (2008) 254–261, <https://doi.org/10.1016/J.JHAZMAT.2007.10.021>.
- [107] G. Crini, H.N. Peindy, F. Gimbert, C. Robert, Removal of C.I. Basic Green 4 (Malachite Green) from aqueous solutions by adsorption using cyclodextrin-based adsorbent: Kinetic and equilibrium studies, *Sep. Purif. Technol.* 53 (2007) 97–110, <https://doi.org/10.1016/J.SEPPUR.2006.06.018>.